

Response Theory via Generative Score Modeling

Ludovico Theo Giorgini,^{1,*} Katherine Deck,^{2,*} Tobias Bischoff,^{3,*} and Andre Souza^{4,*}

¹*Nordita, Royal Institute of Technology and Stockholm University, Stockholm 106 91, Sweden*[†]

²*Climate Modeling Alliance, California Institute of Technology*

³*8362 Solutions, Pasadena, CA, USA*

⁴*Massachusetts Institute of Technology, Cambridge, Massachusetts, United States*

(Dated: July 30, 2024)

We introduce an approach for analyzing the responses of dynamical systems to external perturbations that combines score-based generative modeling with the Generalized Fluctuation-Dissipation Theorem (GFDT). The methodology enables accurate estimation of system responses, including those with non-Gaussian statistics. We numerically validate our approach using time-series data from three different stochastic partial differential equations of increasing complexity: an Ornstein-Uhlenbeck process with spatially correlated noise, a modified stochastic Allen-Cahn equation, and the 2D Navier-Stokes equations. We demonstrate the improved accuracy of the methodology over conventional methods and discuss its potential as a versatile tool for predicting the statistical behavior of complex dynamical systems.

The study of high-dimensional dynamical systems is essential for advancing our understanding of various complex phenomena [e.g., 1–8]. These systems are characterized by numerous interacting degrees of freedom, manifesting feedback mechanisms across spatial and temporal scales. Notable examples of such complexity are observed in climate modeling [e.g., 9], where feedback mechanisms lead to self-sustained spatio-temporal patterns, such as the El Niño Southern Oscillation (ENSO) in the tropical Pacific Ocean, the Asian Monsoon (particularly prominent in South and East Asia), the Indian Ocean Dipole, and the Madden-Julian Oscillation in the Indian and Pacific Oceans [10, 11], among others. Similar complexities and the need to understand feedback mechanisms can be observed in other areas, such as financial markets, [e.g., 12] or neuroscience [e.g., 13, 14].

A central challenge is to characterize the causal relationships among these degrees of freedom without prior knowledge of the underlying evolution laws [15–18]. Causal inference seeks to unambiguously determine whether the behavior of one variable has been influenced by another based on observed time series data. This estimation process is challenging due to the complexity and high dimensionality of these systems [19, 20].

In recent decades, numerous methodologies have been developed to infer causal relationships directly from data [e.g., 21–25], but calculating a system’s response to small perturbations using linear response theory has become a dominant approach [26–28]. This method allows for evaluating responses without actually perturbing the system, leveraging instead the analysis of unperturbed dynamics [29, 30]. It is underpinned by the generalized Fluctuation-Dissipation Theorem (GFDT), an extension of the classical Fluctuation-Dissipation Theorem (FDT) [31]. A central obstacle in applying linear response theory is obtaining the system’s unperturbed invariant distribution, i.e., the distribution of a system’s attractor [32–34].

The invariant distribution is often approximated by as-

suming a multivariate Gaussian distribution ansatz to circumvent this issue [35]. This approximation is reasonable when examining coarse-grained (spatially or temporally) variables or particular physical observables [36, 37]. The limits of this approximation are evident in atmospheric science, where observational data from wind and rainfall exhibit intermittency and other non-Gaussian features [38–41]. Another context for non-Gaussian statistics comes from neuroscience, where the brain’s response to stimuli and the resulting patterns of neural activity display non-Gaussian properties [42].

Our work leverages recent advancements in score-based generative modeling [e.g., 43–47, and follow-on studies] to accurately represent a high-dimensional, nonlinear dynamical system’s invariant distribution via a “score function,” the gradient of the logarithm of a system’s invariant distribution. Score models are used primarily as generative models, i.e., for sampling from the data distribution. Still, they have other applications, such as estimating the dimensionality of the data distribution, see [48]. This study demonstrates another use case beyond sample generation and in an area where machine-learning approaches have not yet been fully utilized: a trained score model can be used to compute response functions using data from dynamical systems.

Using trajectories of the dynamical system, we train a model that approximates the score of the steady-state, or invariant, distribution. The model is a neural network based on spatial convolutions that can capture high-dimensional data distribution statistics (e.g., [49–51]). Like the Gaussian approximation approach, this method only requires time-series data. In this work, we apply the score-based method to three dynamical systems and compare its performance to other standard approaches for computing response functions. This approach outperforms the traditional Gaussian approximation when the underlying system is nonlinear.

Problem description. – We focus on systems described by an evolution equation

$$\partial_t u = F(u) + \xi, \quad (1)$$

where u is the system state, which varies as a function of location in space and time and belongs to a space \mathcal{X} . The function $F : \mathcal{X} \rightarrow \mathcal{X}$ is a map, and ξ is a noise term, which can be taken to be zero to yield a deterministic system. However, we emphasize that the only requirements for applying the methodology here are time-series data, and one does not need to know an underlying evolution law such as Equation (1), which represents systems of both ordinary or partial differential equations.

Introducing a finite-dimensional analog facilitates the connection with computations. When computations are performed on a grid, we use $u_i(t) \equiv u(x_i, t)$ as shorthand to denote the values of u at grid location x_i at time t , where $i \in [1, N^2]$, and N^2 is the number of grid points. Thinking of u_i as the components of a vector in \mathbb{R}^{N^2} , we also use $\vec{u}(t)$ to denote the vector of values u at time t and each grid location x_i . We use similar notation for other functions as well, e.g. if $\vec{f} : \mathbb{R}^{N^2} \rightarrow \mathbb{R}^{N^2}$, then $f_i(u(t))$ denotes the value of $\vec{f}(\vec{u})$ at grid location x_i and time t .

We consider statistically stationary (steady-state) systems with a smooth invariant probability density function $\rho = \rho(u_1, u_2, \dots, u_N^2)$. We will use the GFDT, which is defined in Equation (3), to understand how a small initial perturbation applied at time t alters the expected value of a system's state at a later time $t + \mathcal{T}$, compared to its unperturbed expected state. This relative change in the state after a time \mathcal{T} , $\delta\vec{u}(\mathcal{T})$, has the expectation

$$\langle \delta\vec{u}(\mathcal{T}) \rangle_p \equiv \langle \vec{u}(\mathcal{T}) \rangle_{\mathcal{J}'} - \langle \vec{u} \rangle_\rho, \quad (2)$$

where $\langle \cdot \rangle_\rho$ denotes an expectation over the steady-state attractor distribution ρ , $\langle \cdot \rangle_{\mathcal{J}'}$ denotes an expectation over the joint density $\mathcal{J}'(\vec{u}(t), \vec{v}(t+\mathcal{T}) | \vec{v}(t) = \vec{u}(t) + \delta\vec{u}(t))$, for a fixed perturbation $\delta\vec{u}(t)$ at time t . The ensemble average $\langle \cdot \rangle_p$ is defined by the right-hand side of Equation (2). Below, we will use $\langle \cdot \rangle_{\mathcal{J}}$ to denote an expectation over the joint density $\mathcal{J}(\vec{u}(t), \vec{v}(t+\mathcal{T}) | \vec{v}(t) = \vec{u}(t))$, which can be written as $\mathcal{J}(\vec{u}(t), \vec{u}(t+\mathcal{T}))$.

For a small perturbation to u at grid location j , denoted by δu_j , we wish to quantify the change in the average of u_i at a later time \mathcal{T} (the discrete analog of Equation (2)). The GFDT states that this can be evaluated using a matrix-valued quantity called the response function R_{ij} (we also refer to it as the response matrix) [31] as

$$R_{ij}(\mathcal{T}) \equiv \frac{\langle \delta u_i(\mathcal{T}) \rangle_p}{\delta u_j(0)} = - \langle u_i(\mathcal{T}) s_j(\vec{u}(0)) \rangle_{\mathcal{J}}, \quad (3)$$

where the score function of the steady-state distribution has the usual definition

$$\vec{s} = \nabla \ln \rho. \quad (4)$$

Since we assume that we have access to time-series data, the problem of estimating the response function is thus reduced to estimating the score function $\vec{s}(\vec{u})$ of the steady-state distribution ρ . In deterministic dynamical systems, this invariant distribution is typically singular almost everywhere on the attractor, and it is necessary to introduce Gaussian noise into the system to make ρ sufficiently smooth to apply the GFDT [52] effectively.

If the steady-state distribution is a multivariate Gaussian distribution, the response matrix is given by

$$\mathbf{R}(\mathcal{T}) = \mathbf{C}(\mathcal{T})\mathbf{C}^{-1}(0), \quad (5)$$

where $\mathbf{C}(\mathcal{T})$ is the correlation matrix, with elements $C_{ij}(\mathcal{T}) = \langle u_i(\mathcal{T})u_j(0) \rangle_{\mathcal{J}}$. The property that $R_{ij}(0) = \delta_{ij}$, where δ_{ij} is the Kronecker delta, is a general property that holds for the discrete response matrix, see the Appendix. Constructing the correlation matrix is straightforward, allowing Equation (5) to serve as a convenient method for estimating the response matrix when the underlying steady-state distribution is well-approximated by a Gaussian distribution.

The response function can also be estimated using numerical simulations of the dynamical system. This estimation involves taking an ensemble of initial conditions, perturbing them, evolving the unperturbed and perturbed system forward in time, and then taking an ensemble average. However, this must be repeated for each perturbation of interest, which involves repeated potentially expensive simulations. It also requires knowledge of the equations of motion.

Here, we employ score-based generative modeling, a technique from the machine-learning community, to derive the response function directly from data. Our approach uses denoising score matching and facilitates the parameterization of the dynamical system's attractor score function directly, following methodologies suggested by Song et al. [45, 46]. This approach only requires data and notably does not require approximating the steady-state distribution as Gaussian or require additional numerical simulations for different perturbations.

Score-based modeling for response functions – In most applications of generative modeling, the goal is to generate samples from the data distribution ρ . Generating samples is achieved using a reverse diffusion process, which turns samples from a normal distribution into samples of the data-distribution. This sample generation procedure requires knowledge of the score function from a non-stationary stochastic forward process at each moment in time; one example of such a forward process is

$$\frac{\partial \rho_\tau}{\partial \tau} = \frac{\sigma^2(\tau)}{2} \Delta \rho_\tau, \quad (6)$$

where τ is a pseudo-time, and $\sigma(\tau)$ is a prescribed function [46].

The learning objective is to fit the parameters of a model (often a neural network) to approximate $\vec{s}_\tau =$

$\nabla \ln \rho_\tau$, which appears in the reverse diffusion equation. Knowledge of this function at each diffusion time τ allows one to sample from a Gaussian, evolve the reverse dynamical system, and obtain a sample from the data distribution. What is relevant for response functions is that taking off-the-shelf score-modeling infrastructure allows one to learn \vec{s}_τ , and evaluating this function as $\tau \rightarrow 0$ yields the score of the data distribution (Equation (4)).

We apply the proposed method to three different dynamical systems. We compare the response function computed in this way (Generative) to a response computed by solving the perturbed dynamical system (Dynamical), a response using an analytically derived score function (Analytical) for the systems for which it is possible to derive one, and the response obtained through the Gaussian approximation frequently used in the literature (Gaussian).

Before describing the three systems under study, we note some commonalities. Each represents a stochastic partial differential equation for a scalar variable. We take the spatial domain to be two-dimensional and periodic in each direction. The state field u maps a two-dimensional location into a scalar field, which we represent with a spatial discretization of N^2 degrees of freedom (or pixels, when representing the field as an image). In our study, we used $N = 32$ pixels. We use a coarse resolution so that comparing to the Gaussian approximation is directly tractable as it requires inverting a $32^2 \times 32^2$ matrix. An advection term, $A\partial_x u$, where A is a constant, was added because it introduces a preferred direction of information propagation and, therefore, a direction of causality. The systems differ in their complexity: the first system has Gaussian statistics, the second system is non-Gaussian but has analytically tractable score function, and the last system is non-Gaussian, does not have an analytically tractable score function, and has “hidden dynamics” in the forcing.

An Ornstein-Uhlenbeck Stochastic PDE. – Our first system is an Ornstein-Uhlenbeck (OU) system [53] with spatially correlated noise, [54–57]. The steady-state trajectories of the system exhibit Gaussian statistics, which makes the Gaussian approximation exact, and hence serves as a baseline for testing our method.

Here, we consider a multidimensional version with an advection term and spatially correlated noise:

$$\partial_t u = -\lambda \Sigma u + \kappa \Delta u + A \partial_x u + \epsilon \Sigma^{1/2} \xi, \quad (7)$$

where $u = u(x, y, t)$ is the unknown field which depends on space x, y , and time t , $\Sigma \equiv (1 - \Delta)^{-1}$ is an inverse Helmholtz operator, $A = 2 \times 10^{-2}$, $\epsilon = 2 \times 10^{-3/2}$, $\lambda = 4 \times 10^{-2}$ are constant scalars, and ξ represents space-time noise with covariance

$$\text{Cov}[\xi(x, y, t)] = \delta(x - x', y - y', t - t'), \quad (8)$$

where $\delta(x, y, t)$ is the Dirac delta function. In this case,

an analytically tractable score function is available

$$s(u) = \frac{2}{\epsilon^2} (-\lambda u + \kappa \Delta u - \kappa \Delta^2 u), \quad (9)$$

which doesn’t depend on the advective term $A\partial_x u$.

A modified Allen-Cahn system. – Our second system is the Allen-Cahn system, an example of a reaction-diffusion equation used for modeling phase separation in multi-component systems [see 58, who studied applications to binary alloys]. Reaction-diffusion equations [59] are partial differential equations combining a diffusive term with a (non)linear reaction term. They are commonly used to study pattern formation (e.g., [60–62]) and chemical processes.

We considered a modified version of the Allen-Cahn system to include an advection term and spatially correlated noise, as follows,

$$\partial_t u = \kappa \Delta u - A \partial_x u + \alpha \Sigma (u(1 - u^2)) + \epsilon \Sigma^{1/2} \xi, \quad (10)$$

where $\Sigma, A, \epsilon, u, \xi$ are same as those used in the OU system. We choose parameters $\alpha = 16$, $\kappa = 2.5 \times 10^{-4}$. The system has an analytically tractable score function,

$$s(u) = \frac{2}{\epsilon^2} [\alpha u(1 - u^2) + \kappa(\Delta u - \Delta^2 u)], \quad (11)$$

which, similar to the OU example, doesn’t depend on the advective term $A\partial_x u$. The steady-state trajectories of this system exhibit bimodal statistics, and hence provides an example where the Gaussian approximation to the response function is expected to fail.

For both the OU and Allen-Cahn systems, the analytic score function and the machine-learned score will differ by a constant factor due to the difference between the Kronecker delta and the Dirac delta functions. In both examples, the analytic score function is 32^2 larger. We divide the analytic score by this factor for comparison with the machine-learned score. Refer to the Appendix for the derivation of the analytic score functions.

Navier-Stokes equation. – We next study a version of the 2D Navier-Stokes model as described in [63], where we take the state variable to be the vorticity, u . This system was chosen as a stepping-stone towards the more complex fluids observed in climate systems; however, the vorticity statistics are not strongly non-Gaussian due to the chosen resolution as would be expected from a coarse-grained system, [36]. Hence, we expect good performance from the Gaussian approximation to the response function. The data-generating equation is

$$\partial_t u = \partial_x \psi \partial_y u - \partial_x u \partial_y \psi - A \partial_x u + \mathcal{D}u + \varsigma \quad (12)$$

$$\psi = \Delta^{-1} u \quad (13)$$

$$\mathcal{D}u = -\nu_h \Delta^{-2} u - \nu \Delta^2 u - \nu_0 \int dx dy u \quad (14)$$

where \mathcal{D} is a dissipation operator with constants ($\nu_h = 10^{-2}$, $\nu = 10^{-5}$, $\nu_0 = (2\pi)^{-2}$), $A = \pi$ is a mean advection

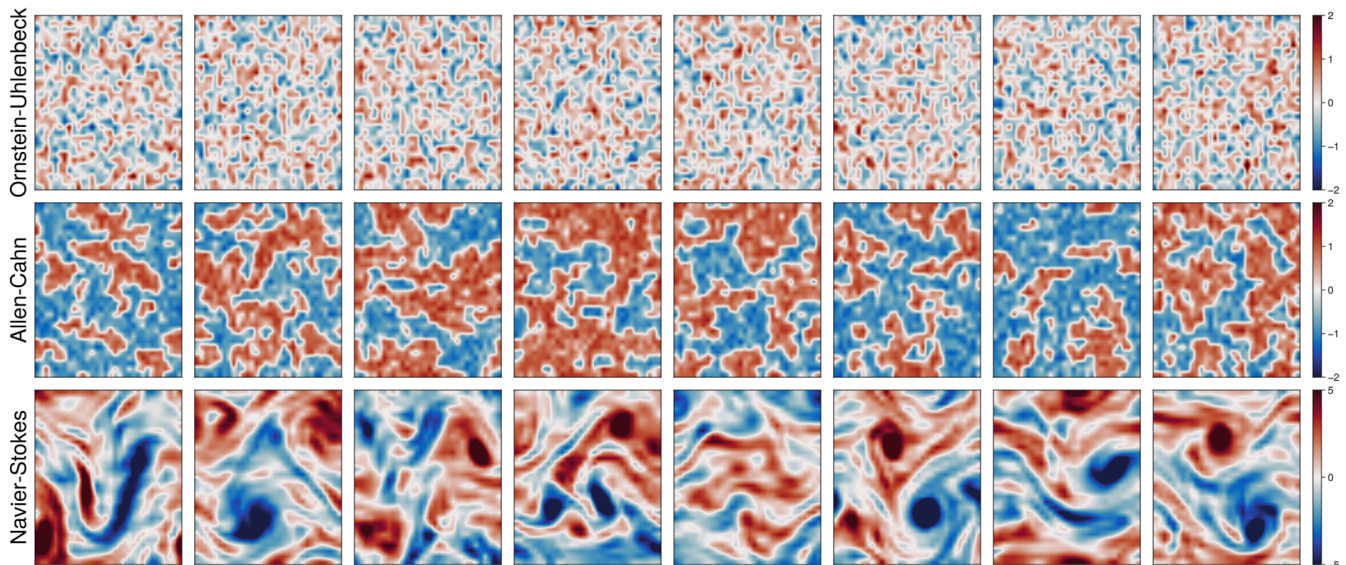


FIG. 1. **Example snapshots of the Three Systems.** In the **top row**, Ornstein-Uhlenbeck PDE, in the **middle row** Allen-Cahn, in the **bottom row** Navier-Stokes

term, and ζ is a random wave forcing from [63]. The random wave forcing introduces hidden dynamics into the system, thus the score function is estimated using only partial state information. The inverse Laplacian is defined to preserve the mean of the original variable.

Results. – We first generate time series data corresponding to Equations (7), (10), and Equation (12). These data are used to compute response functions and the training sets for the score model. To create the training data, we determine autocorrelation times for each and subsample the trajectories to create statistically independent snapshots. Figure (9) shows training data samples of the numerically simulated systems. All details regarding the numerical simulations (time-stepping, spatial discretization), the datasets and the training of the score models are provided in the Appendix, along with an in-depth comparison between data samples generated via numerical simulation of the Allen-Cahn system and those produced using the learned score function of this system through reverse diffusion. Training the neural network took a few hours to a few days to for each score model on a single Nvidia A100.

Owing to the periodic boundary conditions and symmetries of the systems under study, the response matrix elements exhibit translational invariance in the x and y -directions. However, due to the advection term, the response function in the x -direction depends on both the distance and the direction (sign) between pixels while the y -direction only depends on the distance. This invariance implies that the index i in the response matrix R_{ij} can be arbitrarily fixed. We chose $j = 1$ and calculated the response matrix elements along the direction of advection

(denoted by i), as this is the direction information propagation, where we observe a more significant response to perturbations at pixel component $i = 1$. The resulting responses of nearby pixels as a function of time for the three systems are presented in Figure (4). The generative model is consistent with the dynamical response function (“our ground truth”) in all cases. For the OU system, the Gaussian response function also matches the ground truth; this is expected as this system exhibits Gaussian statistics. For the Allen-Cahn system, it is clear that the Gaussian approximation is a poor approximation to the response function. And lastly, for the Navier-Stokes system we see improvement in using the generative score over the Gaussian response, despite the coarse Navier-Stokes system being quasi-Gaussian.

In Figure (5), we compared the error over the entire state field between the Generative, Gaussian, and Analytic (for the systems where it is available) response functions with the Dynamical response function considered as “ground truth” for the three systems as a function of time. We used two different metrics to determine the errors: the L^2 and the L^∞ norm. The L^2 norm measures the average error across all pixels in the domain, providing a sense of the overall error distribution. It is helpful in understanding the general accuracy of the response function over the entire field. On the other hand, the L^∞ norm measures the maximum error at any single pixel, highlighting the worst-case error. This norm is particularly relevant to ensure the minimization of the largest deviations. From the comparison in Figure (5), it is evident that the Generative response function generally outperforms the Gaussian response in the nonlinear cases

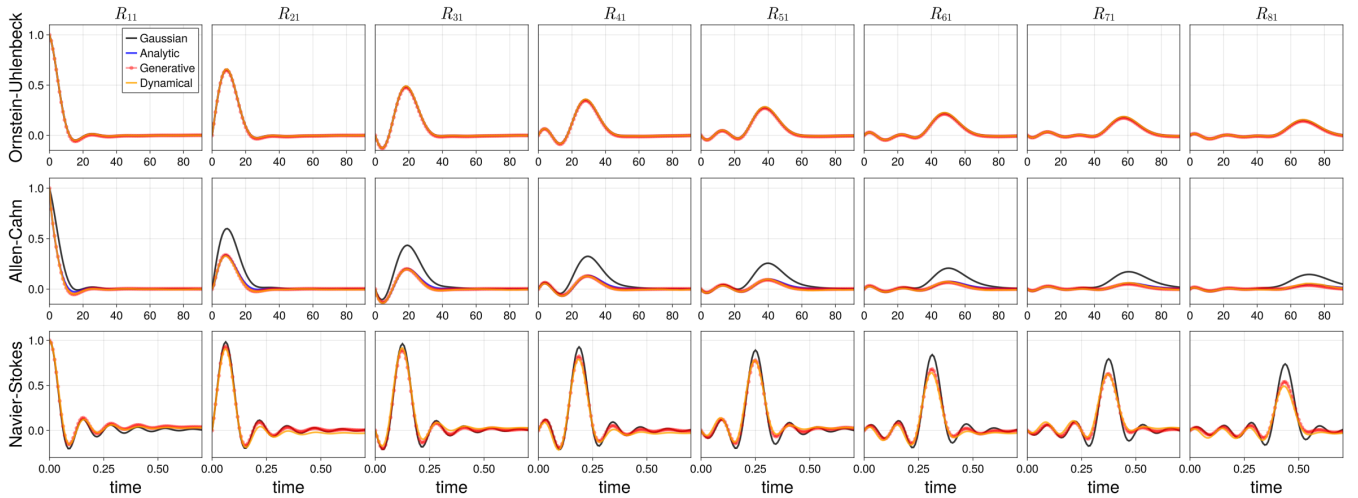


FIG. 2. **Response functions for Three Systems.** The response to a perturbation at the pixel component $i = 1$ is evaluated at various pixel components with coordinates indicated at each panel. All evaluated components align with the advection direction. Responses are computed by integrating the dynamical system (orange lines, “Dynamical”) via Gaussian approximation (black lines, “Gaussian”), using the score function derived from generative modeling (red lines and dots, “Generative”), and using the analytic score function (blue lines, “Analytic”).

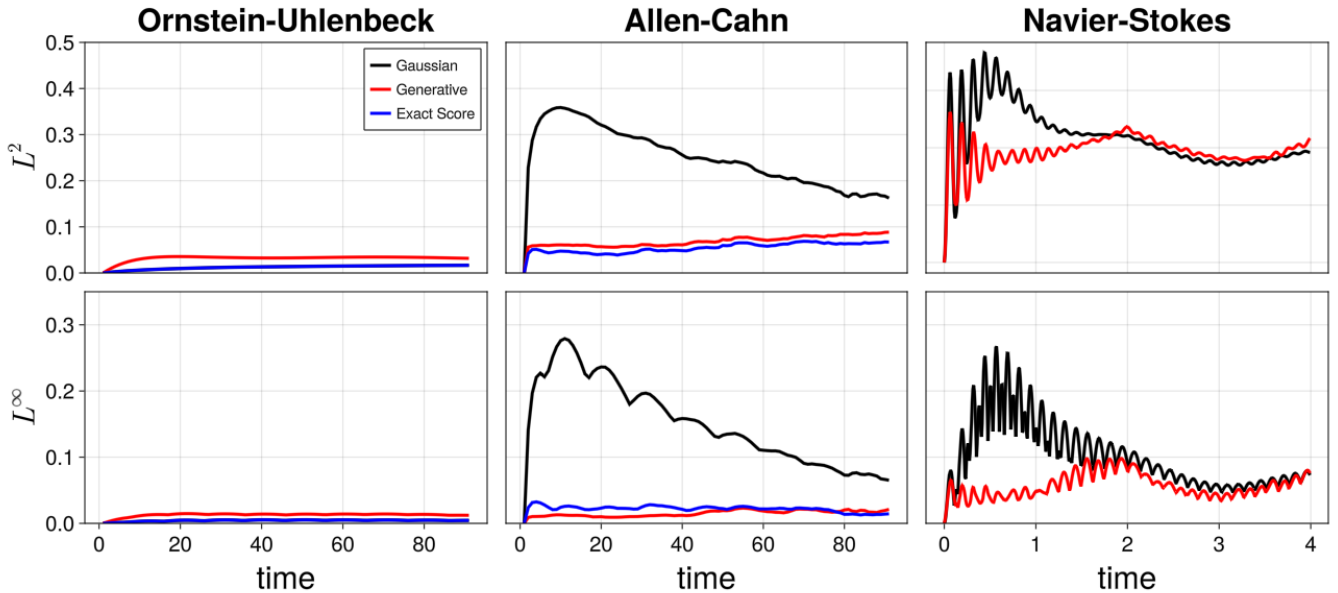


FIG. 3. **Response Function Errors for the Three Systems.** Here, we show both the RMS error and the Infinity Norm error of the Response function as a function of time. Here we use the Dynamic Response function as the “ground truth”. We see that the Generative response (red) generally outperforms the Gaussian response (blue) for the nonlinear cases (Allen-Cahn and Navier-Stokes), especially in the Infinity Norm, and performs similarly for the linear system (Ornstein-Uhlenbeck). The response function computed with the exact score does not have zero error relative to the dynamical response function because of errors introduced in numerical discretization and empirical averaging.

(Allen-Cahn and Navier-Stokes), especially in terms of the L^∞ norm at early to intermediate times. This observation indicates that the Generative model is better at capturing the extreme responses at individual pixels. The Gaussian approximation is exact for the Ornstein-Uhlenbeck

system, which has a Gaussian steady-state distribution, and both the Generative and Gaussian response functions perform similarly.

Drawbacks and Practical Considerations. – While score-based generative models offer a powerful tool for estimating response functions, there are practical challenges. One issue is that training these models requires substantial data or a sufficiently good inductive bias in the parameterized model for the score function. Additionally, setting up and training neural networks can often require significant resources, engineering, and time. Expertise in training neural networks is essential. For example, suppose the data or training time is insufficient, and one is using a U-Net to represent the score function. In that case, the generative response function tends to match the Gaussian approximation’s performance due to the U-Net’s linear bypass connections. A further drawback with any machine-learning method is the lack of performance “out-of-sample”; indeed, in the Appendix, we demonstrate that the score model for the Allen-Cahn system performs poorly when evaluated on data dissimilar from the training data.

For many applications, especially those mentioned in the introduction, several additional steps may need to be taken to apply the methods from this study effectively. One crucial step is the incorporation of domain-specific knowledge into the design of the neural network architecture. This will significantly improve the model’s inductive bias and alleviate the data burden. Additionally, domain-specific challenges such as non-stationarity or incomplete state information must be incorporated [64]. This is particularly salient for climate data, which exhibits diurnal, seasonal, and longer timescale variations [65, 66]. As always, it is crucial to validate the trained model with known benchmarks or analytical solutions.

Conclusions. – In this study, we use score-based diffusion models to compute response functions, offering a purely data-driven method to calculate accurate response functions. We validated this approach on a system with Gaussian statistics (Ornstein-Uhlenbeck) and two dynamical systems with more complex distributions: a reaction-diffusion equation (Allen-Cahn) and the Navier-

Stokes equations. The former is a class of SPDEs that have applications across biology, chemistry, and physics, and the latter is a system exhibiting some of the characteristics of more complex fluids like the Earth’s atmosphere or ocean. We compared the response function of these systems computed in multiple ways: using an *analytic* expression for the score, using the *generative* score function, using a *dynamical* approach by introducing perturbations to initial conditions and solving the equations of motion, and using a *Gaussian* approximation. In this case, we found that the Gaussian response function over-predicted the response to neighboring perturbations and that the generative response function agreed well with both the dynamical and analytical response functions. Compared with the Gaussian response, the RMSE of the generative response function had significantly reduced error. This suggests that score-based models are a useful tool for studying system response functions.

The code utilized in this work is publicly available for further study and replication at: https://anonymous.4open.science/r/PrivateGenLRT-052E/generate/allen_cahn_model.jl. We used the publicly available codebase <https://github.com/Clima/CliMAgen.jl> as the backbone for training the models.

The authors would like to thank three anonymous reviewers for their suggestions which greatly enhanced the scope, quality, and presentation of the letter. LTG gratefully acknowledges support from the Swedish Research Council (Vetenskapsradet) Grant No. 638-2013-9243. KD acknowledges support from Schmidt Sciences and the Cisco Foundation. AS acknowledges support from Schmidt Sciences through the Bringing Computation to the Climate Challenge, an MIT Climate Grand Challenge Project. AS thanks Fabrizio Falasca and Glenn Flierl for their invaluable suggestions in improving preliminary versions of this work. TB acknowledges the support of the community at Livery Studio and useful discussions with Bryan Riel on generative modeling.

Generalized Fluctuation Dissipation Theorem

For a system in statistical equilibrium, the Generalized Fluctuation Dissipation Theorem (GFDT) relates perturbations to system dynamics and the invariant measure associated with the system. Although the perturbations are considered to act only on initial conditions, the resulting theory can also be applied when continuous forcing is used. As such, the GFDT can be used to calculate response functions. These are the appropriate objects to use when predicting expected (relatively) small changes in system dynamics. Applications of the theorem include statistical mechanics, causality relations, and climate change.

Variable Names and Assumptions

We assume a (finite-dimensional) dynamical system of the form

$$\dot{\vec{u}} = \vec{f}(\vec{u}) + \epsilon \vec{\xi} \quad (15)$$

where \vec{f} is the deterministic part of the dynamics and $\vec{\xi}$ is delta-correlated in time (state-independent) white-noise. We further assume that the dynamical system admits a unique and differentiable steady-state probability distribution $\rho(\vec{u})$ that solves the steady-state Fokker-Plank equation

$$\nabla \cdot \left(\vec{f}\rho - \frac{\epsilon^2}{2}\nabla\rho \right) = 0. \quad (16)$$

In this section, we abuse notation and let subscripts on the vector \vec{u} denote different random variables. For example, \vec{u}_0 is a random variable associated with the time $t = 0$, and $\vec{u}_\mathcal{T}$ is a random variable associated with $t = \mathcal{T}$.

The transition probability from a past state to a future state is denoted by $\rho(\vec{u}_\mathcal{T}|\vec{u}_0)$ and this probability is the solution to the forward evolution of the Fokker-Plank equation starting with initial density $\rho(\vec{u}, 0) = \delta(\vec{u} - \vec{u}_0)$, e.g.

$$\mathcal{L}\bullet \equiv \nabla \cdot \left(\vec{f}\bullet - \frac{\epsilon^2}{2}\nabla\bullet \right) \quad (17)$$

$$\rho(\vec{u}_\mathcal{T}|\vec{u}_0) \equiv \exp(\mathcal{T}\mathcal{L})\delta(\vec{u} - \vec{u}_0) \quad (18)$$

where \mathcal{L} is the Fokker-Plank operator and $\exp(\mathcal{T}\mathcal{L})$ is the Perron-Frobenius operator at time \mathcal{T} , i.e., the operator exponential of \mathcal{L} over timescale \mathcal{T} . Thus $\vec{u}_\mathcal{T}$ is correlated with \vec{u}_0 over short times. We also let

$$\rho(\vec{u}_\mathcal{T}, \vec{u}_0) \equiv \rho(\vec{u}_\mathcal{T}|\vec{u}_0)\rho(\vec{u}_0) \quad (19)$$

denote the joint probability distribution between \vec{u}_0 and $\vec{u}_\mathcal{T}$.

We have the relations

$$\rho(\vec{u}) = \lim_{\mathcal{T} \rightarrow \infty} \rho(\vec{u}_\mathcal{T}|\vec{u}_0) = \int d\vec{u}_0 \rho(\vec{u}|\vec{u}_0)\rho(\vec{u}_0) \quad (20)$$

where the middle equality states that the invariant measure $\rho(\vec{u})$ is unique and the last equality states that $\rho(\vec{u})$ is an eigenvalue of the Perron-Frobenius operator $\rho(\vec{u}|\vec{u}_0)$ with eigenvalue 1.

An observable g maps our state \vec{u} to a scalar value. This observable can be any (linear/nonlinear) functional of the state \vec{u} . We are often concerned with the evolution of different observables of our system.

Definition of System Perturbations

An operational definition of “system perturbation” (in the text we denoted this as the “Dynamical response”) is

1. Choose a fixed (small in magnitude) perturbation vector $\vec{\epsilon}$
2. Choose an observable g
3. Draw an initial condition drawn from the system steady-state distribution
4. Evolve two trajectories, one with initial condition \vec{u}_0 and the other with initial condition $\vec{u}_0 + \vec{\epsilon}$. Use the same sequence of noise realizations in each case if the system is stochastic.
5. Compute the difference between the observable g in the perturbed and unperturbed trajectory at each moment in time starting from $t = 0$.
6. Repeat 2-4 for many initial conditions drawn from the steady state distribution and average the result.

The above sequence of steps is considered the “left-hand side” of the GFDT.

If we treat the “left-hand side” of the GFDT as the “Langevin” version of GFDT, the “right-hand side” is the “Fokker-Plank” definition followed by approximations. We first consider the average value of an observable of the unperturbed trajectory. As is done in the Dynamical response, we first draw an initial condition from the distribution $\rho(\vec{u}_0)$, then evolve our trajectory forward in time so that the distribution in the end is $\rho(\vec{u}_\mathcal{T}|\vec{u}_0)$. We are interested in the average value of the observable at time \mathcal{T} ; thus, the observable is evaluated at $g(\vec{u}_\mathcal{T})$. Together, this yields the unperturbed average

$$\int d\vec{u}_0 d\vec{u}_\mathcal{T} \rho(\vec{u}_0)\rho(\vec{u}_\mathcal{T}|\vec{u}_0)g(\vec{u}_\mathcal{T}), \quad (21)$$

which simplifies to

$$\int d\vec{u}_0 d\vec{u}_\mathcal{T} \rho(\vec{u}_0) \rho(\vec{u}_\mathcal{T}|\vec{u}_0) g(\vec{u}_\mathcal{T}) = \int d\vec{u}_\mathcal{T} \rho(\vec{u}_\mathcal{T}) g(\vec{u}_\mathcal{T}) = \langle g \rangle \quad (22)$$

from our assumptions that there is a unique steady-state distribution.

The perturbed version follows from the same logic. As is done in the Dynamical response, we first draw an initial condition from the distribution $\rho(\vec{u}_0)$, then evolve our trajectory forward in time from a perturbed version of our initial condition, $\vec{u}_0 + \vec{\varepsilon}$, so that the distribution in the end is $\rho(\vec{u}_\mathcal{T}|\vec{u}_0 + \vec{\varepsilon})$. Thus, our perturbed trajectory is

$$\langle g \rangle_p = \int d\vec{u}_0 d\vec{u}_\mathcal{T} \rho(\vec{u}_0) \rho(\vec{u}_\mathcal{T}|\vec{u}_0 + \vec{\varepsilon}) g(\vec{u}_\mathcal{T}). \quad (23)$$

The difference between the two yields the Fokker-Plank version

$$\langle \delta g \rangle = \langle g \rangle_p - \langle g \rangle \quad (24)$$

This equation is the starting point for deriving the Generalized Fluctuation Dissipation Theorem.

Derivation with State-Dependent Perturbations

We will derive the Generalized Fluctuation Dissipation Theorem, in line with Appendix A of [29], and further generalize to the case where the perturbation is allowed to be state-dependent. The average change in an observable g with respect to a state-dependent perturbation $\vec{\varepsilon}(\vec{u}_0)$ to an initial condition \vec{u}_0 is given by

$$\langle \delta g_\mathcal{T} \rangle \equiv \int d\vec{u}_0 d\vec{u}_\mathcal{T} g(\vec{u}_\mathcal{T}) \rho(\vec{u}_0) [\rho(\vec{u}_\mathcal{T}|\vec{u}_0 + \vec{\varepsilon}(\vec{u}_0)) - \rho(\vec{u}_\mathcal{T}|\vec{u}_0)], \quad (25)$$

where $\vec{\varepsilon}$ is an infinitesimal of magnitude ε . If we assume that we have a steady state distribution, e.g., $\int d\vec{u}_0 \rho(\vec{u}_\mathcal{T}|\vec{u}_0) \rho(\vec{u}_0) = \rho(\vec{u}_\mathcal{T})$, we have

$$\int d\vec{u}_0 d\vec{u}_\mathcal{T} g(\vec{u}_\mathcal{T}) \rho(\vec{u}_0) \rho(\vec{u}_\mathcal{T}|\vec{u}_0) = \int d\vec{u}_0 d\vec{u}_\mathcal{T} g(\vec{u}_\mathcal{T}) \rho(\vec{u}_0) \rho(\vec{u}_\mathcal{T}|\vec{u}_0) \quad (26)$$

$$= \int d\vec{u}_\mathcal{T} g(\vec{u}_\mathcal{T}) \rho(\vec{u}_\mathcal{T}) \quad (27)$$

$$= \langle g \rangle \quad (28)$$

where the last quantity is the ensemble average of g .

We now focus on simplifying the expression

$$\int d\vec{u}_0 d\vec{u}_\mathcal{T} g(\vec{u}_\mathcal{T}) \rho(\vec{u}_0) \rho(\vec{u}_\mathcal{T}|\vec{u}_0 + \vec{\varepsilon}(\vec{u}_0)). \quad (29)$$

First, make the change of variable

$$\vec{v}_0 = \vec{u}_0 + \vec{\varepsilon}(\vec{u}_0) \quad (30)$$

which implies

$$\vec{u}_0 = \vec{v}_0 - \vec{\varepsilon}(\vec{u}_0) \Rightarrow \vec{u}_0 = \vec{v}_0 - \vec{\varepsilon}(\vec{v}_0 - \vec{\varepsilon}(\vec{u}_0)). \quad (31)$$

To first order, we then have

$$\vec{u}_0 = \vec{v}_0 - \vec{\varepsilon}(\vec{v}_0) + \mathcal{O}(\varepsilon^2) \quad (32)$$

with ε denoting the perturbation strength of $\vec{\varepsilon}$. The resulting differential is

$$d\vec{u}_0 = \det(\mathbb{I} - \varepsilon \mathbf{J}) d\vec{v}_0 \quad (33)$$

where $\varepsilon\mathbf{J}$ is the Jacobian of $\vec{\varepsilon}$, $\nabla\vec{\varepsilon} = \varepsilon\mathbf{J}$, and \mathbb{I} is the identity matrix. The expression can be simplified using Jacobi's formula for the derivative of the determinant to yield

$$\det(\mathbb{I} - \varepsilon\mathbf{J}) \approx 1 - \text{trace}(\varepsilon\mathbf{J}) = 1 - \nabla \cdot \vec{\varepsilon} \quad (34)$$

The change of coordinates does not shift the limits of integration, which is over all of space. Thus we have

$$\int d\vec{u}_0 d\vec{u}_{\mathcal{T}} g(\vec{u}_{\mathcal{T}}) \rho(\vec{u}_0) \rho(\vec{u}_{\mathcal{T}} | \vec{u}_0 + \vec{\varepsilon}(\vec{u}_0)) \quad (35)$$

$$= \int d\vec{v}_0 d\vec{u}_{\mathcal{T}} (1 - \nabla \cdot \vec{\varepsilon}) g(\vec{u}_{\mathcal{T}}) \rho(\vec{v}_0 - \vec{\varepsilon}) \rho(\vec{u}_{\mathcal{T}} | \vec{v}_0) \quad (36)$$

$$\approx \langle g \rangle - \int d\vec{v}_0 d\vec{u}_{\mathcal{T}} g(\vec{u}_{\mathcal{T}}) (\vec{\varepsilon} \cdot \nabla \ln \rho(\vec{v}_0) + \nabla \cdot \vec{\varepsilon}(\vec{v}_0)) \rho(\vec{v}_0, \vec{u}_{\mathcal{T}}) + \mathcal{O}(\varepsilon^2) \quad (37)$$

Our final expression then simplifies to

$$\langle \delta g_{\mathcal{T}} \rangle = - \int d\vec{u}_0 d\vec{u}_{\mathcal{T}} g(\vec{u}_{\mathcal{T}}) (\vec{\varepsilon}(\vec{u}_0) \cdot \nabla \ln \rho(\vec{u}_0) + \nabla \cdot \vec{\varepsilon}(\vec{u}_0)) \rho(\vec{u}_0, \vec{u}_{\mathcal{T}}) \quad (38)$$

where we took the liberty to replace the dummy variable \vec{v}_0 with \vec{u}_0 . In total, we need to calculate the correlation of the function $\vec{\varepsilon} \cdot \nabla \ln \rho + \nabla \cdot \vec{\varepsilon}$ at time 0, with the observable g at time $0 + \mathcal{T}$, for each \mathcal{T} of interest. Under the assumption of a statistically steady state, we observe that each time t of our ensemble of simulations comes from the same steady-state distribution ρ . Thus we can correlate the observable g at time $t + \mathcal{T}$ with $\vec{\varepsilon} \cdot \nabla \ln \rho + \nabla \cdot \vec{\varepsilon}$ at time t .

Simplifications

In the text, the perturbation $\vec{\varepsilon}$ is not state-dependent, in which case the change in the observable simplifies to

$$\langle \delta g_{\mathcal{T}} \rangle = -\vec{\varepsilon} \cdot \int d\vec{u}_0 d\vec{u}_{\mathcal{T}} g(\vec{u}_{\mathcal{T}}) \nabla \ln \rho(\vec{u}_0) \rho(\vec{u}_0, \vec{u}_{\mathcal{T}}). \quad (39)$$

We observe that the vector quantity

$$\vec{R}_g(\mathcal{T}) = \int d\vec{u}_0 d\vec{u}_{\mathcal{T}} g(\vec{u}_{\mathcal{T}}) \nabla \ln \rho(\vec{u}_0) \rho(\vec{u}_0, \vec{u}_{\mathcal{T}}) \quad (40)$$

is independent of the perturbation choice $\vec{\varepsilon}$. The typical response function makes several choices for the observable g by choosing a set of observables g_i where $g_i(\vec{u}_0) = \langle \hat{e}_i, \vec{u}_0 \rangle$, so that the set of vectors $\vec{R}_{g_i}(\mathcal{T})$ are combined together into a single response matrix \mathcal{R}_{ij} . Once one has access to \mathcal{R}_{ij} , the response of any linear functional g to a small perturbation can be computed. The continuous analog of the Response matrix is the Response kernel, where the i, j indices represent different locations in the domain.

Further Uses of Response Functions

Once one has the Response matrix \mathcal{R}_{ij} , it is possible to understand how a system behaves with respect to a continuous forcing by convolving with the response matrix. For example, if

$$\dot{\vec{u}} = \vec{f}(\vec{u}) + \vec{h}(t) + \vec{\xi} \quad (41)$$

$$\dot{\vec{v}} = \vec{f}(\vec{v}) + \vec{\xi} \quad (42)$$

then $\langle u_i - v_i \rangle(t) = \int_0^t d\mathcal{T} \sum_j \mathcal{R}_{ij}(t - \mathcal{T}) h_j(\mathcal{T})$ where \vec{u} and \vec{v} have the same initial condition drawn from the invariant distribution of the \vec{v} system, u_i, v_i, h_i denotes the i 'th component of $\vec{u}, \vec{v}, \vec{h}$, respectively, and the same sequence of noise ξ is used in both system. In other words, the ensemble average of the difference between the two dynamical systems is given by convolution with respect to the response function.

The Response Function Using the Gaussian Approximation

In this section, we derive the response function using the Gaussian approximation presented in Equation (5) of the manuscript. The Gaussian approximation consists of approximating the unperturbed steady-state distribution ρ with a multivariate Gaussian distribution

$$\rho_G(\vec{u}) = \frac{1}{(2\pi)^{N^2/2}(\det \Sigma)^{1/2}} \exp\left(-\frac{1}{2}\vec{u}^T \Sigma^{-1} \vec{u}\right), \quad (43)$$

with Σ the correlation matrix $C(0)$ calculated for $t = 0$. Using Equation (4) of the manuscript, we can write the score function as

$$\vec{s}_G(\vec{u}) = -\Sigma^{-1} \vec{u}. \quad (44)$$

The response function then becomes

$$\mathbf{R}_G(\mathcal{T}) = \langle \vec{u}(\mathcal{T}) \otimes \vec{u}(0) \rangle_{\mathcal{J}} \Sigma^{-1} = C(t) C^{-1}(0). \quad (45)$$

Derivation of the Score Function for Potential Systems

For a stochastic dynamical system with correlated noise,

$$\dot{\vec{u}} = \vec{f}(\vec{u}) + \Sigma^{1/2} \vec{\xi} \quad (46)$$

the corresponding Fokker-Planck equation is

$$\partial_t \rho + \nabla \cdot \left(\vec{f} \rho - \frac{1}{2} \Sigma \nabla \rho \right) = 0. \quad (47)$$

We observe that if $\vec{f} = -\frac{1}{2} \Sigma \nabla V$ for some potential function $V(\vec{u})$ then the solution steady-state Fokker-Planck equation is

$$\rho \propto e^{-V}, \quad (48)$$

from whence the score function is $\vec{s}(\vec{u}) = -\nabla V$. A generalization of this observation is if $\vec{f} = -\frac{1}{2} \Sigma \nabla V + \vec{g}$ where \vec{g} satisfies the following property

$$\nabla \cdot (\vec{g} e^{-V}) = 0. \quad (49)$$

As a comment, we can always decompose the deterministic component \vec{f} in this manner if we take $V \equiv \ln \rho$ with ρ as the steady state distribution and *define* $\vec{g} \equiv \vec{f} + \frac{1}{2} \Sigma \nabla V$. The gradient of the potential term, ∇V , corresponds to the time-reversible part of the dynamics, and \vec{g} corresponds to the time-irreversible component.

A sufficient condition that can often be satisfied is

$$\nabla \cdot \vec{g} = 0 \text{ and } \nabla V \cdot \vec{g} = 0. \quad (50)$$

The first restriction states that the function \vec{g} can't concentrate probability, and the latter restriction states that \vec{g} can only move the probability on iso-surfaces of the steady state probability density. The advection term in the two potential systems of the manuscript satisfied Equation 50.

For example, consider the linear stochastic differential equation

$$\frac{d}{dt} \begin{bmatrix} x \\ y \end{bmatrix} = \begin{bmatrix} -1 & 1 \\ 0 & -1 \end{bmatrix} \begin{bmatrix} x \\ y \end{bmatrix} + \begin{bmatrix} \xi_1 \\ \xi_2 \end{bmatrix} \quad (51)$$

$$= \underbrace{\begin{bmatrix} -0.8 & 0.4 \\ 0.4 & -1.2 \end{bmatrix} \begin{bmatrix} x \\ y \end{bmatrix}}_{-\frac{1}{2} \Sigma \nabla V} + \underbrace{\begin{bmatrix} -0.2 & 0.6 \\ -0.4 & 0.2 \end{bmatrix} \begin{bmatrix} x \\ y \end{bmatrix}}_{\vec{g}} + \begin{bmatrix} \xi_1 \\ \xi_2 \end{bmatrix} \quad (52)$$

where the function \vec{g} satisfies Equation 50,

$$V = [x \ y] \begin{bmatrix} 0.8 & -0.4 \\ -0.4 & 1.2 \end{bmatrix} \begin{bmatrix} x \\ y \end{bmatrix}, \text{ and } \Sigma = \begin{bmatrix} 1 & 0 \\ 0 & 1 \end{bmatrix}. \quad (53)$$

See [67] for examples corresponding to Langevin dynamics.

Similar considerations apply to Stochastic PDEs. We can connect them to the finite-dimensional case through a spatial numerical discretization of the underlying PDE.

The Modified Allen-Cahn Equation

The potential function for the modified Allen-Cahn system is given by the following integral

$$\mathcal{V}[u] = \frac{2}{\epsilon^2} \int \left[\frac{\alpha}{4} (1 - u^2)^2 + \frac{\kappa}{2} (|\nabla u|^2 + |\Delta u|^2) \right] d\vec{u}, \quad (54)$$

where the parameters are defined in the main text. In steady-state, the probability density (or Gibbs measure) is given by [68]

$$\rho(u) \propto \exp(-\mathcal{V}), \quad (55)$$

which yields the score function

$$s(u) = -\frac{\delta \mathcal{V}}{\delta u} = \frac{2}{\epsilon^2} [\alpha u(1 - u^2) + \kappa(\Delta - \Delta^2)u]. \quad (56)$$

We comment that the fluctuation-dissipation relation at time $t = 0$ is

$$-\int \mathcal{D}[u] u s(u) \rho(u) = \delta(\mathbf{x} - \mathbf{y}), \quad (57)$$

which differs from the discrete version by δ_{ij} to $\delta(\mathbf{x} - \mathbf{y})$. Here, we used a path integral notation for the previous equation. The presence of the correlated noise yields dynamics of the form

$$\partial_t u = -\frac{\epsilon^2}{2} \Sigma \frac{\delta \mathcal{V}}{\delta u} + \epsilon \Sigma^{1/2} \xi. \quad (58)$$

Adding in an advection term, as was done in the manuscript,

$$\partial_t u = -\frac{\epsilon^2}{2} \Sigma \frac{\delta \mathcal{V}}{\delta u} - U \partial_x u + \epsilon \Sigma^{1/2} \xi. \quad (59)$$

does not affect the steady-state distribution.

To see that the advection term does not affect the steady-state distribution only requires changing reference frames to one with a velocity U and using the translational invariance of the probability density. Alternatively, one can directly show via the Fokker-Plank equation that the advection term satisfies Equation 50. The reason the advection term vanishes is two-fold: the first is that the trace of the advection operator is zero, the second observation is that the inner product vanishes,

$$\int (U \partial_x u) \frac{\delta \mathcal{V}}{\delta u} d\vec{u} = 0, \quad (60)$$

in a periodic domain for a constant velocity U . For more details on the topic, see [68]. The same procedure can be applied to the Ornstein-Uhlenbeck system by replacing the nonlinear term with a linear one. With the Ornstein-Uhlenbeck system, it is possible to write down the score function for all diffusion times analytically.

Practical Considerations

Bridging the gap between theories and data requires several practical considerations. The discrete identity

$$\langle u_i s_j(\vec{u}) \rangle = -\delta_{ij} \quad (61)$$

will often not be satisfied due to approximation errors. This identity follows from the calculation

$$\langle u_i s_j(\vec{u}) \rangle = \int_{\Omega} d\vec{u} \rho(\vec{u}) u_i s_j(\vec{u}) = \int_{\Omega} d\vec{u} \rho(\vec{u}) u_i \partial_{u_j} \ln \rho(\vec{u}) \quad (62)$$

$$= \int_{\Omega} d\vec{u} \rho(\vec{u}) u_i \frac{\partial_{u_j} \rho(\vec{u})}{\rho(\vec{u})} = - \int_{\Omega} d\vec{u} u_i \partial_{u_j} \rho(\vec{u}) \quad (63)$$

$$= - \int_{\Omega} d\vec{u} (\partial_{u_j} u_i) \rho(\vec{u}) = - \int_{\Omega} d\vec{u} \delta_{ij} \rho(\vec{u}) \quad (64)$$

$$= -\delta_{ij} \int_{\Omega} d\vec{u} \rho(\vec{u}) = -\delta_{ij} 1 \quad (65)$$

There are three primary sources of approximation error in satisfying this discrete identity.

1. Ensemble averages are often approximated using empirical averages.
2. The score function is approximated using a parameterized model with finite data and training time.
3. The generative score function is the score function of the data convolved with a multivariate Gaussian of small width when using a denoising score loss.

With sufficient data and a sufficiently flexible parametric model, the first two errors are mitigated but not eliminated. The latter error is fundamental to estimating a score function using the denoising score loss but is often negligible compared to the first two errors. Thus, we will focus on the first two sources of approximation error and will return to the third afterward.

Correction Procedure

In practice, with sufficient data, Equation (61) becomes

$$-\langle u_i s_j(\vec{u}) \rangle \approx -\sum_{\omega=1}^N u_i^\omega s_j(\vec{u}^\omega) = \delta_{ij} - \Xi_{ij} \quad (66)$$

where we have approximated the ensemble average with an empirical average with the superscript ω denoting different ensemble members, and the matrix Ξ is a small “error” matrix. The score function at diffusion time $\tau = 0$, used in the manuscript, corrected this issue by using a modified score to satisfy the discrete identity, similar to how the Gaussian approximation satisfies the discrete identity.

We modify the score function by composing it with an additional linear operator to satisfy Equation (61),

$$\vec{\zeta} \equiv \vec{s}(\mathbb{I} - \Xi)^{-1} \quad (67)$$

This modified score satisfies the discrete identity since

$$-\sum_{\omega=1}^N u_i^\omega \zeta_j(\vec{u}^\omega) = -\left(\sum_{\omega=1}^N u_i^\omega s_j(\vec{u}^\omega)\right) (\mathbb{I} - \Xi)^{-1} = (\mathbb{I} - \Xi)(\mathbb{I} - \Xi)^{-1} = \mathbb{I} \quad (68)$$

We could have also used

$$\vec{\zeta}_2 \equiv (\mathbb{I} - \Xi)^{-1} \vec{s} \text{ or } \vec{\zeta}_3 \equiv \frac{1}{2} (\vec{s}(\mathbb{I} - \Xi)^{-1} + (\mathbb{I} - \Xi)^{-1} \vec{s}) \quad (69)$$

as the definition of the modified score, but experimentation yielded little difference between the different choices.

Although we used the corrected score function ζ from Equation (67) in all computations in the manuscript, including those involving the analytic score function, it was not strictly necessary for the fidelity of any computations; however, using the correction procedure here, greatly decreased the number of epochs necessary to obtain an improved result over the Gaussian approximation. See Section .

Uncorrected Score Results

We justify the statement from the previous section by showing results with the uncorrected score function values. It is worth keeping in mind that the Gaussian approximation that is often used in the literature satisfies the identity Equation (61); thus, the baseline comparison will be more favorable towards the Gaussian model at short times even when compared to the “exact” score function; however, the generative model’s performance remains better than the Gaussian counterpart for the nonlinear cases.

We see that in Figure 4 the results are relatively unchanged with respect to the results in the main manuscript with respect to the strongest responses in the system. In the Allen-Cahn system we see that the analytic score function underperforms with respect to the generative model, which we justify as a combination of two effects: the generative score is more tailored to the data-distribution and the ensemble averaging yields errors in computing the response function.

We quantify the error in Figure 5. We see that the generative model has a higher error than the Analytic error in the L^2 sense for the Ornstein-Uhlenbeck and Allen-Cahn systems. The generative model has enhanced performance

with respect to the Gaussian approximation in the Allen-Cahn system but, due to the accumulation of errors in many of the grid-points, the L^2 error is comparable to the Navier-Stokes Gaussian approximation error. For the L^∞ error we see that the generative model outperforms the Gaussian approximation in the nonlinear regime and is comparable (but less performant) in the linear regime.

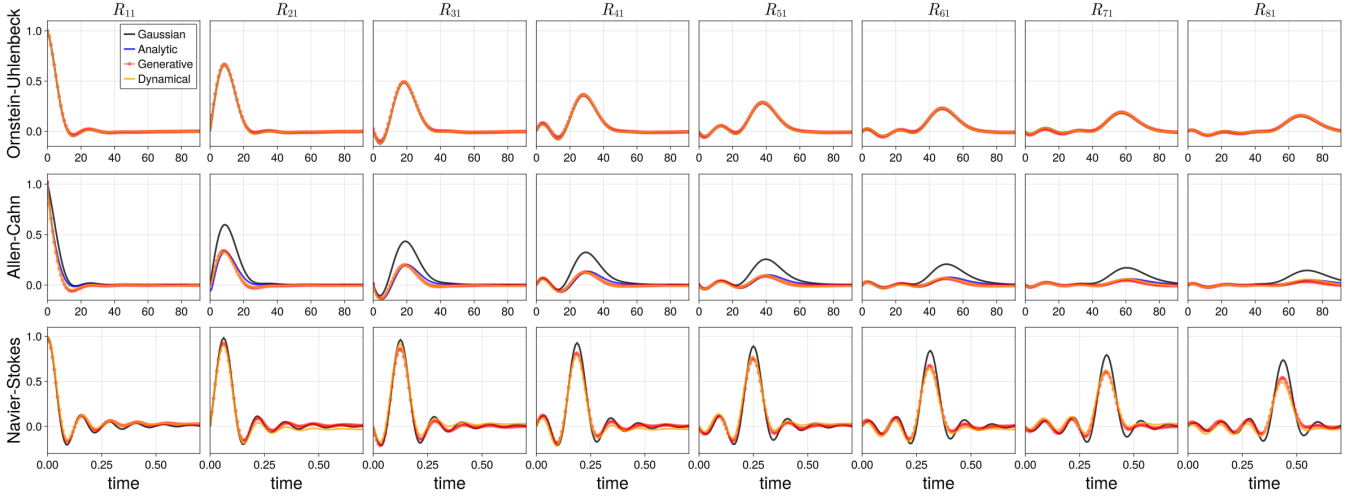


FIG. 4. **Response functions for Three Systems.** The response to a perturbation at the pixel component $i = 1$ is evaluated at various pixel components with coordinates indicated at each panel. All evaluated components align with the advection direction. Responses are computed by integrating the dynamical system (orange lines, “Dynamical”) via Gaussian approximation (black lines, “Gaussian”), using the score function derived from generative modeling (red lines and dots, “Generative”), and using the analytic score function (blue lines, “Analytic”). The “Dynamical” response is taken as the “ground truth”.

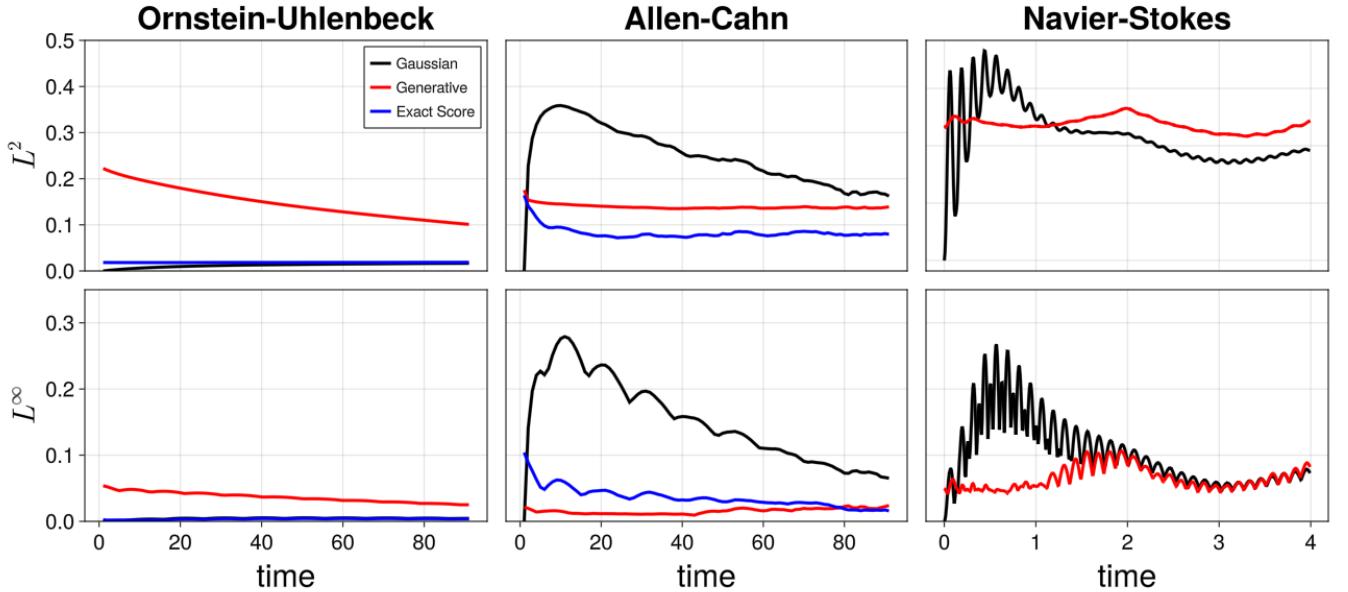


FIG. 5. **Response Function Errors for the Three Systems.** Here, we show both the RMS error and the Infinity Norm error of the Response function as a function of time. Here, we use the Dynamic response function as the “ground truth”. We see that the Generative response (red) generally outperforms the Gaussian response (black) for the nonlinear cases (Allen-Cahn and Navier-Stokes), especially in the Infinity Norm, and performs similarly for the linear system (Ornstein-Uhlenbeck).

A Comment on Generative Score function

The generative score function does not find the score function of the data distribution but instead finds the score function convolved with an independent multivariate normal whose width is σ_{min} due to the use of the denoising score loss. In principle, we can instead calculate covariances of the “noised” data. Thus, we can add to our multivariate random noise \vec{Z} . This modification, in principle, allows us to satisfy the identity, Equation (61), to a higher fidelity; however, this procedure is useful only if the true system response is robust in the $\sigma_{min} \rightarrow 0$ limit.

Adding small noise to the data has the additional benefit of regularizing the distribution. Thus, if the distribution lies in a lower dimensional subspace, convolving it with a multivariate Gaussian makes it occupy the full space. When performing an estimate in the Gaussian case, this has the consequence that the covariance matrix becomes

$$C(\vec{u} + \vec{Z}, \vec{u} + \vec{Z}) = C(\vec{u}, \vec{u}) + \sigma_{min}^2 \mathbb{I} \quad (70)$$

where C is the spatial covariance operator and \mathbb{I} is the identity matrix.

An alternative is to train a Neural network for $\sigma_{min} = 0$ separately using a different loss function.

The Effect of Shifts and Normalizations on Response Functions

It is common to shift and normalize the data so that

$$\tilde{u} = au + b \quad (71)$$

where a and b are constants. Regarding response functions, we note that the response function for u and \tilde{u} is exactly the same. To see this denote the distributions for u and \tilde{u} by $\rho_1(u)$ and $\rho_2(\tilde{u})$. The response matrix is

$$\langle u_i \partial_{u_j} \ln \rho_1 \rangle = \langle (a^{-1} \tilde{u}_i - a^{-1} b) \partial_{a^{-1} \tilde{u}_j} \ln \rho_2 \rangle = \langle \tilde{u}_i \partial_{\tilde{u}_j} \ln \rho_2 \rangle. \quad (72)$$

It is easier to see that the above relation holds from the empirical estimate of the expected value. Thus, one can correlate the score function of the shifted and scaled data distribution with the shifted and scaled data to get the response function for the unshifted and scaled data distribution. More complex data transformations require further analysis.

Denoising Score Matching

In this section, we focus on estimating the score function of the attractor of a dynamical system, as defined in Equation (3), through a denoising score matching training procedure often used in generative modeling [45, 46, and follow-on studies]. This process approximates the score with a trainable function and subsequently optimizes its parameters. In principle, this could be achieved by minimizing an explicit score-matching loss function in which a trainable function is compared to the exact score. However, the true score function is generally unknown.

To overcome this problem, we perturb the data across a continuum of noise scales as is done in [44, 45, 69] by using a forward diffusion process governed by the stochastic differential equation (SDE; [46]).

$$d_\tau \vec{u} = \vec{\xi}_\tau, \quad (73)$$

where τ is a diffusion time not to be confused with the physical time of the dynamical system from the previous section. Here, we employ a notation common in the physical sciences, rather than using the Wiener process differential $d\vec{W}$. Note that we consider a discretized version of the continuous scalar field u on an $N \times N$ grid, such that the dimensionality of the discretized u (denoted with the vector arrow) is N^2 . Furthermore, $\vec{\xi}_\tau$ is a N^2 -dimensional zero-mean random normal vector with diagonal covariance matrix and variance g_τ^2 for all components of $\vec{\xi}_\tau$. The initial condition for Equation (73), at time $\tau = 0$, is drawn from the steady-state distribution (e.g., the attractor):

$$\vec{u}_0 \sim \rho(u_1, \dots, u_{N^2}), \quad (74)$$

where ρ corresponds here to the distribution of the discretized system in steady state. The solution of Equation (73) at any diffusion time τ , \vec{u}_τ , follows a multivariate Gaussian distribution

$$\vec{u}_\tau \sim \mathcal{N}(\vec{u}_0, \sigma_\tau^2 \mathbb{I}), \quad (75)$$

with diagonal covariance matrix $\sigma_\tau^2 \mathbb{I}$ governed by the variance

$$\sigma_\tau^2 = \int_0^\tau g_{\tau'}^2 d\tau'. \quad (76)$$

In particular, at $\tau = 0$ we have that $\sigma_0 = 0$ and therefore \vec{u}_0 is a sample from the data distribution. For generative modeling and this form of forward diffusion, the function g_τ is often chosen to grow exponentially with diffusion time τ so that at a final time $\tau = 1$ the variance is much larger than the original scale of the data points [e.g., 46]. As a result, the distribution of \vec{u}_1 can be approximated as

$$\vec{u}_1 \approx \mathcal{N}(\vec{0}, \sigma_1^2 \mathbb{I}). \quad (77)$$

This is referred to as the ‘‘variance-exploding’’ form of the forward diffusion process [46]. As noted in the main text, there is a corresponding equation for the density which approaches a Gaussian distribution as $\tau \rightarrow \infty$. This choice ensures that the memory of the initial condition in the diffusion process is lost, mapping points in the observed space \vec{u}_0 to points in the latent space \vec{u}_1 drawn from a known distribution independent of the source data; the independence of the latent distribution from the data is what allows for easy generation of new samples by solving the reverse process.

Since the score function \vec{s}_τ of the density of the discrete system changes smoothly with τ , it is easier to learn using the denoising score matching loss [46]. We choose a suitable function approximator (e.g., a neural network) and train it with the denoising score matching loss given by

$$\mathcal{L}(\theta) = \mathbb{E} \left[\lambda(\tau)^2 \left\| \vec{s}_\theta(\vec{u}_0 + \sigma_\tau \vec{\epsilon}, \tau) + \frac{\vec{\epsilon}}{\sigma_\tau} \right\|^2 \right], \quad (78)$$

where $\lambda(\tau)$ is an optional weighting factor, θ indicate a set of parameters, and the expectation \mathbb{E} is a shorthand for $\mathbb{E}_{\tau \sim \mathcal{U}(\tau_{\min}, 1), \vec{u}_0 \sim \rho, \vec{\epsilon} \sim \mathcal{N}(\vec{0}, \mathbb{I})}$ [46]. Previous work in [46] has found that limiting the expectation over time to a minimum value of $\tau_{\min} \ll 1$ is necessary as the loss function diverges at $\tau = 0$, where $\sigma_0 = 0$. Furthermore, the loss function in Equation (78) is slightly modified in training: we rewrite the score network as

$$\vec{s}_\theta(\vec{u}, \tau) = \frac{\vec{f}_\theta(\vec{u}, \tau)}{\sigma_\tau}, \quad (79)$$

where $\vec{f}_\theta(\vec{u}, \tau)$ is a trainable function and σ_τ is the conditional standard deviation of the forward diffusion process. This allows the function \vec{f}_θ to target a quantity of order unity [e.g., 44, 45, 70].

Having trained the score function \vec{s}_θ we can use it to estimate the score of the steady-state (e.g., the attractor) ρ to use it as a drop-in score estimator within the context of Equation (3) of the manuscript. This is accomplished by setting $\tau = \tau_{\min} \ll 1$ as input to the trained score model so that we have

$$\vec{s}(u) \approx \vec{s}_\theta(\vec{u}, 0) \approx \vec{s}_\theta(\vec{u}, \tau_{\min}), \quad (80)$$

where the first approximation is due to representation error in s_θ or imperfect training, and the second is due to evaluating that function at $\tau = \tau_{\min}$ and not at $\tau = 0$.

Choosing a weighting function $\lambda(\tau)$

As noted, the score function $\vec{s}_\theta(\vec{u}, \tau)$ is most often used in the literature to generate synthetic data samples using the reverse process of Equation (73) [71], and hence $\vec{s}_\theta(\vec{u}, \tau)$ is required for all τ . However, in this work, we are primarily interested in the score network evaluated at $\tau = 0$. This can be controlled with the $\lambda(\tau)$ weighting function.

For the Ornstein-Uhlenbeck and Allen-Cahn systems, we adopt the standard parameterization of $\lambda(\tau) = \sigma(\tau)$ [44, 45, 70], which has been found to produce high-quality samples. However, for the Navier-Stokes case, we found it important to emphasize the diffusion times closest to zero in the loss function; in this case, we chose $\lambda(\tau) = \delta(\tau - \tau_{\min})\sigma(\tau)$. Note that different weighting schedules can strongly affect the quality of generated samples [e.g., 72]. This is important because the samples can be used to validate the model when no other source of truth is available.

The noising schedule

The prescribed noising schedule $\sigma(\tau)$ remains to be specified. Using the Variance Exploding (VE) schedule [46], we have the noising process

$$g_\tau \equiv \sigma_{\min} \left(\frac{\sigma_{\max}}{\sigma_{\min}} \right)^\tau \sqrt{2 \log \left(\frac{\sigma_{\max}}{\sigma_{\min}} \right)} \quad (81a)$$

$$\sigma_\tau^2 \equiv \sigma_{\min}^2 \left[\left(\frac{\sigma_{\max}}{\sigma_{\min}} \right)^{2\tau} - 1 \right], \quad (81b)$$

where σ_{\min} and σ_{\max} are scalar parameters determining the shape of the variance with time. Suitable values of the σ_{\max} can be computed from the data [70], e.g., σ_{\max} is given by the largest pairwise L_2 -distance in the dataset. From these expressions, it is clear that $\sigma_0 = 0$, i.e. that \vec{u}_0 coincides with the data. As noted above, however, $\sigma_0 = 0$ leads to divergences in the loss function and instability in training (see e.g. [46]), so we restrict the diffusion time to $1 \geq \tau \geq \tau_{\min}$.

For the Navier-Stokes case, we use a weighting function that only includes $\tau = \tau_{\min}$ as that is all we really need to generate good estimates for the score function at small τ . We used a value of $\sigma_{\min} = 10^{-3}$ and τ_{\min} as

$$\tau_{\min} = \log \left(\sqrt{2} \right) / \log \left(\sigma_{\max} / \sigma_{\min} \right), \quad (82)$$

which implies that the score function learned at this time is the score function of the data with a small amount of Gaussian noise added. Note that the parameter σ_{\max} cancels out at $\tau = \tau_{\min}$ and therefore does not affect the results for this case. For the Ornstein-Uhlenbeck and Allen-Cahn systems, we set $\sigma_{\min} = 0.01$, and $\sigma_{\max} = 14$.

Score Model Training Details

In this section, we describe the training procedure for the score models. Dataset sizes and time to train for the architecture we used were provided in the main text. All of what is described below is a summary of standard methods for the field. We found that no hyperparameter tuning was required for training the models using the Ornstein-Uhlenbeck and Allen-Cahn data sets, but varying the kernel size and noising schedule improved results for the Navier-Stokes data. Prior experience with training these models was invaluable.

Architecture

The network architecture used is based on a U-Net [49]. An initial ‘‘lifting’’ layer preserves the size of the image, while increasing the number of channels. Three downsampling layers follow, which reduce the size of the image each by a factor of 2, while increasing the number of channels. Eight residual blocks follow, which preserve image size and channel number. Three upsampling layers then increase image size, each by a factor of two, and decrease the number of channels. A final projection layer projects down to a single channel while preserving image size. Two-dimensional spatial convolutions are used in each layer. For both the Ornstein-Uhlenbeck and Allen-Cahn data sets, convolutional kernels of size 3 x 3 pixels were used throughout. For the Navier-Stokes data set, a higher capacity network was required; we found that kernels of size 31x31, 31x31, 15x15, and 7x7 worked well for the lifting and three downsampling layers; we found also that dropout was required, and used a value of 0.5. In all cases, the channel increases are $1 \rightarrow 32 \rightarrow 64 \rightarrow 128 \rightarrow 256$. All convolutions used respect the periodicity of the system using periodic padding. As is standard in score-based diffusion modeling, the diffusion time τ is embedded using a Gaussian Fourier projection [73]; we used an embedding dimension of 256. We made use of the publicly available Julia code <https://github.com/CliMA/CliMAgen.jl/> for the score-model training and sampling. All other architecture parameters were left at their defaults.

We found that doubling the number of channels in the U-net architecture to $1 \rightarrow 64 \rightarrow 128 \rightarrow 256 \rightarrow 512$ did not substantially improve results. Furthermore, increasing the kernel sizes in the Allen-Cahn and Ornstein-Uhlenbeck process did not improve the results. Using dropout decreased training time when using larger kernel sizes, but was unnecessary for the smaller kernel sizes.

Training

Data processing

All snapshots were normalized as described in Section . We used batch sizes of 128 for the Allen-Cahn and Ornstein-Uhlenbeck data, and 1024 for the Navier-Stokes data. We trained for 200 passes over the data for the OU and Allen-Cahn datasets, and 1600 for the Navier-Stokes dataset.

The Ornstein-Uhlenbeck system used 12,800 snapshots, the Allen-Cahn system used 25,600, and the Navier-Stokes data used 131,072 snapshots. Approximately 20% of this data was withheld during training to create a “test” set. We did not thoroughly explore whether or not we could use less data and achieve the same fidelity of results.

Optimization

We used the default optimization configuration of CliMAgen.jl. This is an Adam optimizer with $\epsilon = 10^{-8}$, $\beta_1 = 0.9$, and $\beta_2 = 0.999$ [74]. We normalize the gradient at each step, and use a warmup period of 5000 gradient updates to linearly increase the learning rate to 2×10^{-4} from 0.

Hyperparameter Sensitivity

Here, we aim to provide a condensed parameter sensitivity study by showcasing errors in computing response functions for two extremes of training a neural network architecture for the score of the Navier-Stokes system. The first architecture has kernel sizes of 3x3, 3x3, 3x3, and 3x3 for the lifting and three downsampling layers and channel increases of $1 \rightarrow 32 \rightarrow 64 \rightarrow 128 \rightarrow 256$. Furthermore, it is trained without dropout on the default loss function for all diffusion times $[\tau_{\min}, 1]$ with $\sigma_{\min} = 10^{-3}$ and $\sigma_{\max} = 10$. The second architecture has kernel sizes of 31x31, 31x31, 15x15, and 7x7 for the lifting and three downsampling layers and channel increases of $1 \rightarrow 64 \rightarrow 128 \rightarrow 256 \rightarrow 512$. Furthermore, it is trained with a dropout of 0.5 on a modified loss function for diffusion times $[\tau_{\min}, \tau_{\min}]$ with $\sigma_{\min} = 10^{-3}$. This architecture is twice the size used in the main manuscript due to the channel sizes and produces lower errors than that reported in the main manuscript. The first architecture took 30 seconds per epoch, and the second architecture took 5 minutes per epoch on an Nvidia A100 GPU.

We see the response function errors of using the raw and corrected score functions as a function of simulated time and number of epochs used for training the network over the same dataset in Figures 6 and 7. We overlay the Gaussian error in both figures for comparison. In all cases, we see that using the corrected generative score improves the error in computing the response function compared to the generative score without correction (raw). Furthermore, we see that in both architectures, once sufficiently trained, the generative model outperforms the Gaussian response, especially with regard to the most extreme responses. From Figure 6, we see that the raw generative response does not match the performance of the Gaussian approximation for the default network and loss functions for any number of training epochs, which we attribute to a neural network architecture with insufficient complexity to capture the score function of the Navier-Stokes system over all diffusion times. On the other hand, we see in Figure 7, with a larger architecture and different loss function, the raw generative model outperforms the Gaussian approximation and nearly matches that of the corrected generative model for the latter epochs. Early in training, we see that the corrected generative response matches that of the Gaussian response.

Model Validation

For both the Ornstein-Uhlenbeck and Allen-Cahn data sets, we validated the learned score function by numerically solved the reverse SDE using an Euler-Maruyama timestepper with initial condition \vec{u}_1 drawn from the approximate latent distribution at $\tau = 1$, e.g., $\vec{u}_1 \sim \mathcal{N}(\vec{0}, \sigma_{\max}^2 \mathbb{I})$ [46]. The diffusion time interval $\tau \in [1, \tau_{\min}]$ was split into 250 equally spaced steps.

We generated samples using the reverse diffusion sampling strategy. Various statistical metrics (power spectra, the first four moments of the pixel value distribution) were computed using these synthetic samples and using samples from the real training data in order to assess the quality of the model. We ascertained that the power spectra and moments computed with both sample sets agreed within the uncertainties due to finite sample size, and we also visually inspected the loss curves to assess whether the training was converged.

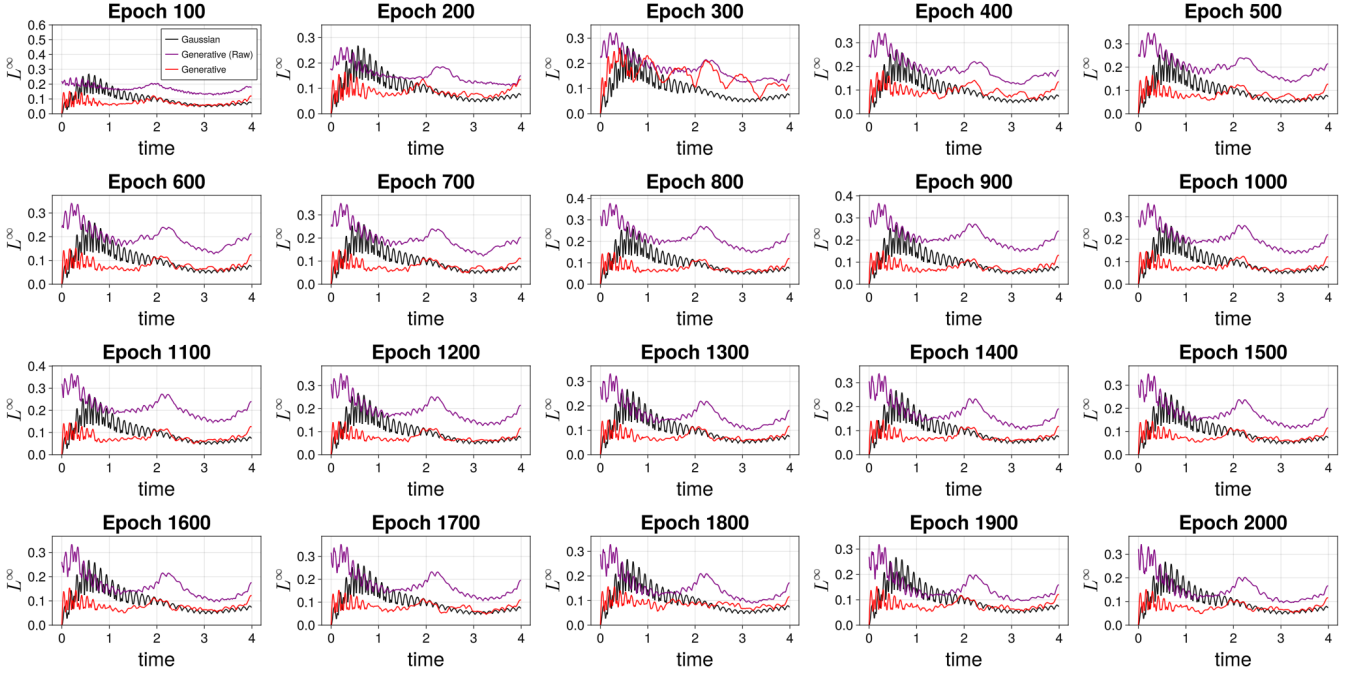


FIG. 6. Response Function Errors for the Navier-Stokes System as the Training Proceeds for a Small Network. We show the Gaussian Response (black) as a baseline for comparison with the Raw Generative Model (purple) and the corrected Generative model (red) for several epochs of training.

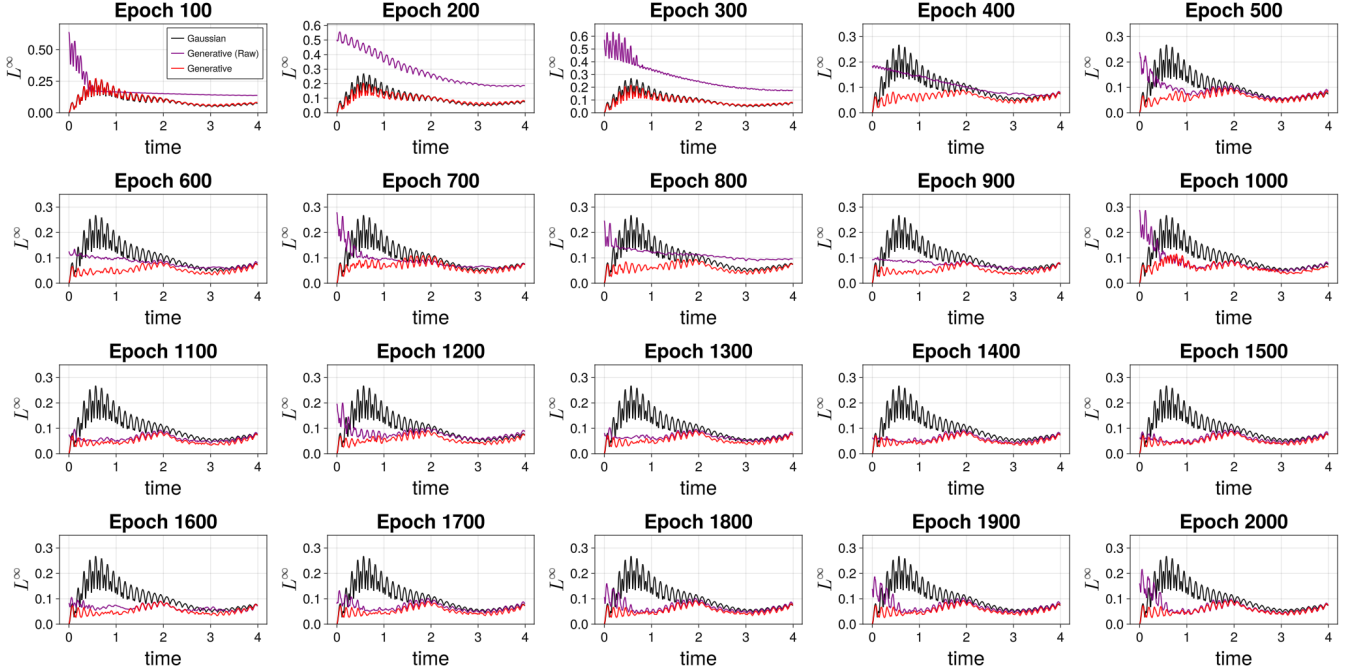


FIG. 7. Response Function Errors for the Navier-Stokes System as Training Proceeds for a Larger Network. We show the Gaussian Response (black) as a baseline for comparison with the Raw Generative Model (purple) and the corrected Generative model (red) for several epochs of training.

This validation was not possible for the Navier-Stokes trained model, due to our choice of weighting function of $\lambda(\tau)$ - see Section .

In all cases, we validate the score at $\tau = \tau_{\min}$ via response functions, as noted in the main text, and against analytic expectation if available.

Further Studies with the Allen-Cahn Equation

Figure 8 shows an example trajectory of the modified Allen-Cahn equation. As we proceed further in time, we see that the pattern shifts to the right (as given by the advection term) and changes according to the stochastic dynamics.

Example training data samples and the steady-state pixel distribution of the numerically simulated system are shown in the upper row of Figure (9). The machine-learned method generates new samples in the bottom row of Figure (9) and the corresponding steady-state pixel distribution. The machine-learned score function can generate samples similar to the original distribution. We compare the steady-state pixel distributions of both the generated fields and data samples to the Gaussian distribution defined by the data’s mean and variance (as used in the Gaussian approximation) in the rightmost panels of Figure (9).

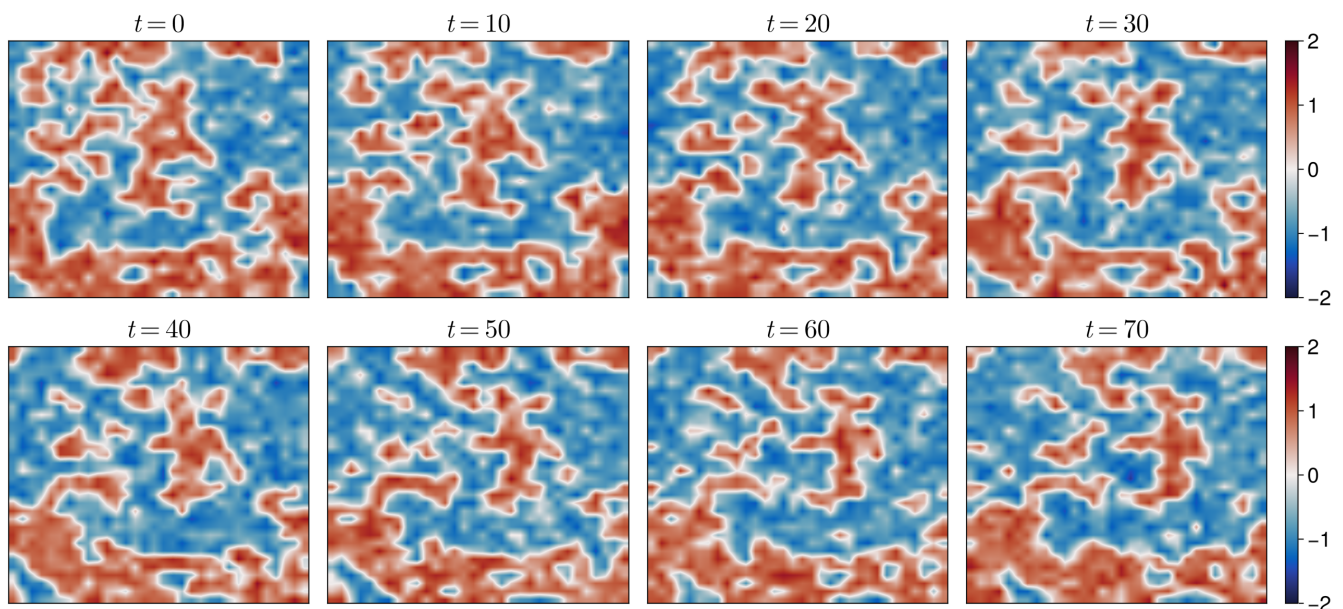


FIG. 8. **Example trajectory of the Allen-Cahn equation.** Time progresses from 0 to 70 time units from top left to bottom right. We used approximately uncorrelated snapshots - sampled every 100 units of time - in training. Both the periodicity of the solution at the boundaries and the advection (to the right) are also visible in the trajectory.

Since we have access to the analytic score function, we have an alternative method of assessing the generative model’s fidelity. We evaluate Equation (56) (scaled by $1/32^2$) and the generative score for several choices of fields u in Figure (10). We test both on data similar to what the neural network has seen before (but not in the training set) and fields far from the original attractor distribution. When applying the score function to a constant field (left panel) for a choice of amplitude (such as $u = 0, u \pm 1, u = 0.5$, etc.), we obtain a cubic polynomial for the analytic score and a similar shape for the generative score, albeit with a significantly smaller amplitude. When evaluated on a smooth field (top three panels on the right), the generative score predicts the “rings”. Still, it cannot obtain the center and mistakenly assigns different values to that region. Lastly, we see excellent agreement between the analytic and predictive score functions when evaluated on data similar to the steady-state distribution of the Allen-Cahn equation (bottom three panels on the right). We reemphasize that the neural network was only exposed to images of the steady-state distribution. In summary, the neural network reproduces the score function when evaluated on data similar to what it has been exposed to. However, the neural network produces quantitatively incorrect answers with similar qualitative features for significantly out-of-sample functions.

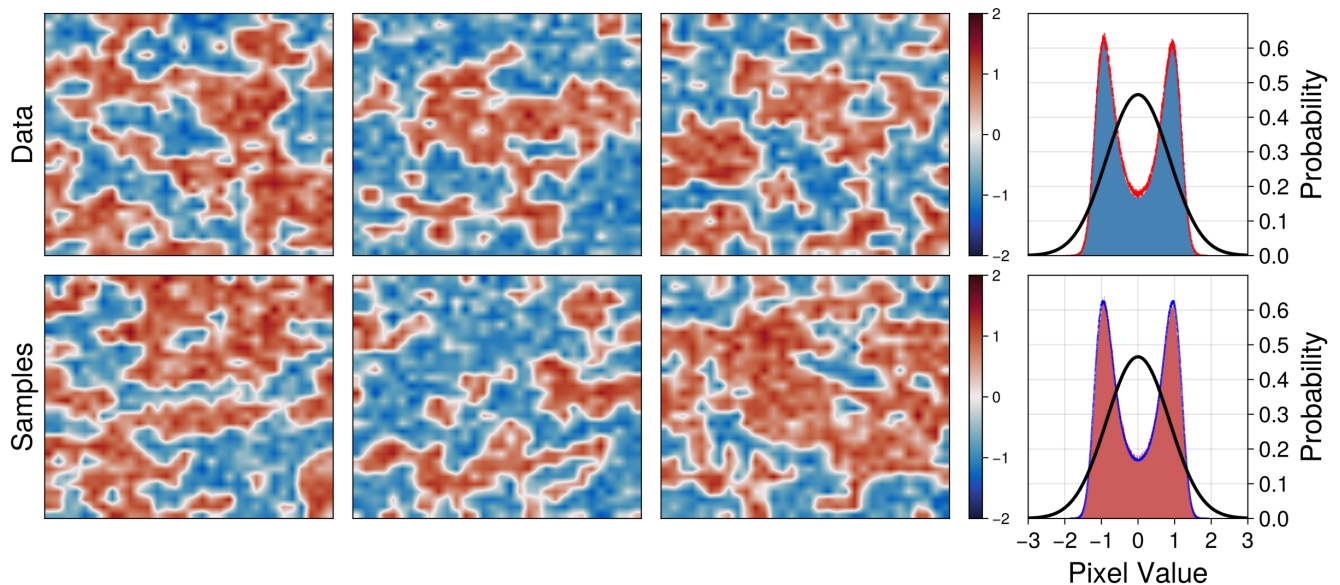


FIG. 9. **Example snapshots and steady-state pixel distribution of the solution to the Allen-Cahn equation.** In the **top row**, we show the results of a numerical simulation of the Allen-Cahn equation) on a domain of size $2\pi \times 2\pi$ using 32×32 pixels; in the **bottom row**, we show samples generated via the learned score function using reverse diffusion [46]. The rightmost column shows the corresponding pixel distributions, where the blue and red lines indicate the equivalent distributions from the top and bottom, respectively. The black line shows the Gaussian approximation fitted to the bimodal pixel distribution.

Colormaps of the System Responses

In this section, we present the colormaps of $R_{ij}(t)$, defined in Equation (3) of the manuscript, for different values of t and for each of the three systems studied: Ornstein-Uhlenbeck (Figure 11), Allen-Cahn (Figure 12), and Navier-Stokes (Figure 13). These figures illustrate how each system responds to a small perturbation applied at the index $(1, 1)$, showing how the perturbation propagates over time.

The use of periodic boundary conditions on all sides allowed us to apply a circular shift to the image pixels. This method repositions the perturbed pixel to the center. For visual clarity, a shorter color range compared to Figure 2 in the manuscript is used.

Numerical Solution of the PDEs in the Manuscript

We use a Fourier spectral method for the spatial discretization for all three systems in the manuscript [75]. The temporal discretization was implemented via a Runge-Kutta 4 scheme for the deterministic dynamics accounting for the noise term after the final Runge-Kutta stage. The timestep size was $\Delta t = 1/32$ for the Ornstein-Uhlenbeck and Allen-Cahn equations and $\Delta t = 1/128$ for the Navier-Stokes system. No dealiasing was used for any of the nonlinear terms of the simulation. All systems were evolved in a domain of size $[0, 2\pi)^2$ and took less than an hour to generate the dataset. The Navier-Stokes system was implemented on an A100 GPU and the Ornstein-Uhlenbeck and Allen-Cahn equations were run on a single core of a CPU with an Apple M1 chip, both with the Julia programming.

The Navier-Stokes system was discretized by averaging the conservative and advective forms of the discrete system. The random-wave forcing in [63] co-evolves a random variable φ alongside the Navier-Stokes equations as,

$$\dot{\varphi} = \xi \quad (83)$$

and the forcing on the right-hand side of the Navier-Stokes equation was

$$\tilde{\zeta} = \mathcal{F}^{-1} \left[F \sum_{i=1}^N a_i \exp(i\varphi_i) \right] \quad \text{and} \quad \zeta = \text{real} \left(\tilde{\zeta} - \nu_f \int \tilde{\zeta} \, dx \, dy \right) \quad (84)$$

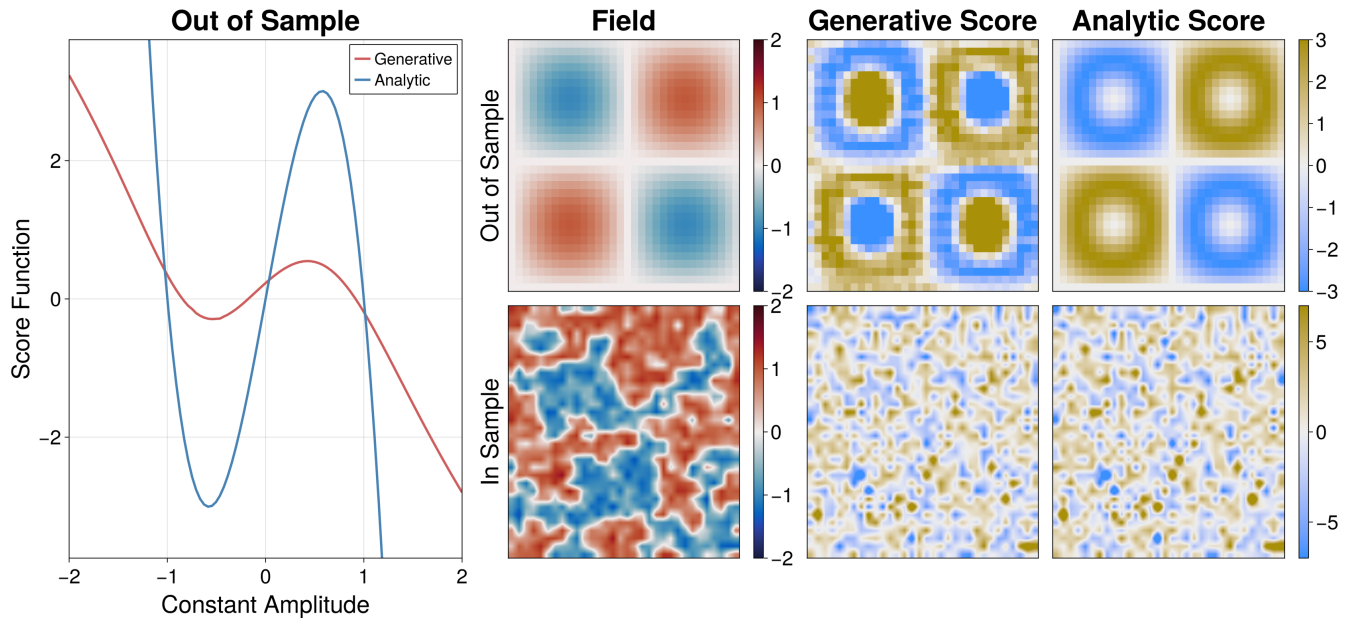


FIG. 10. **Score function evaluation.** Here, we evaluate the analytic score function and the generative score function for several cases. In the leftmost plot, we show the evaluation of a constant function with amplitude given by the horizontal axis. On the right, we show the evaluation of the score function in two separate cases: The first is on the function $\sin(x)\sin(y)$, and the second is a data sample in the test set. Color ranges are the same for fields in which comparisons can be made.

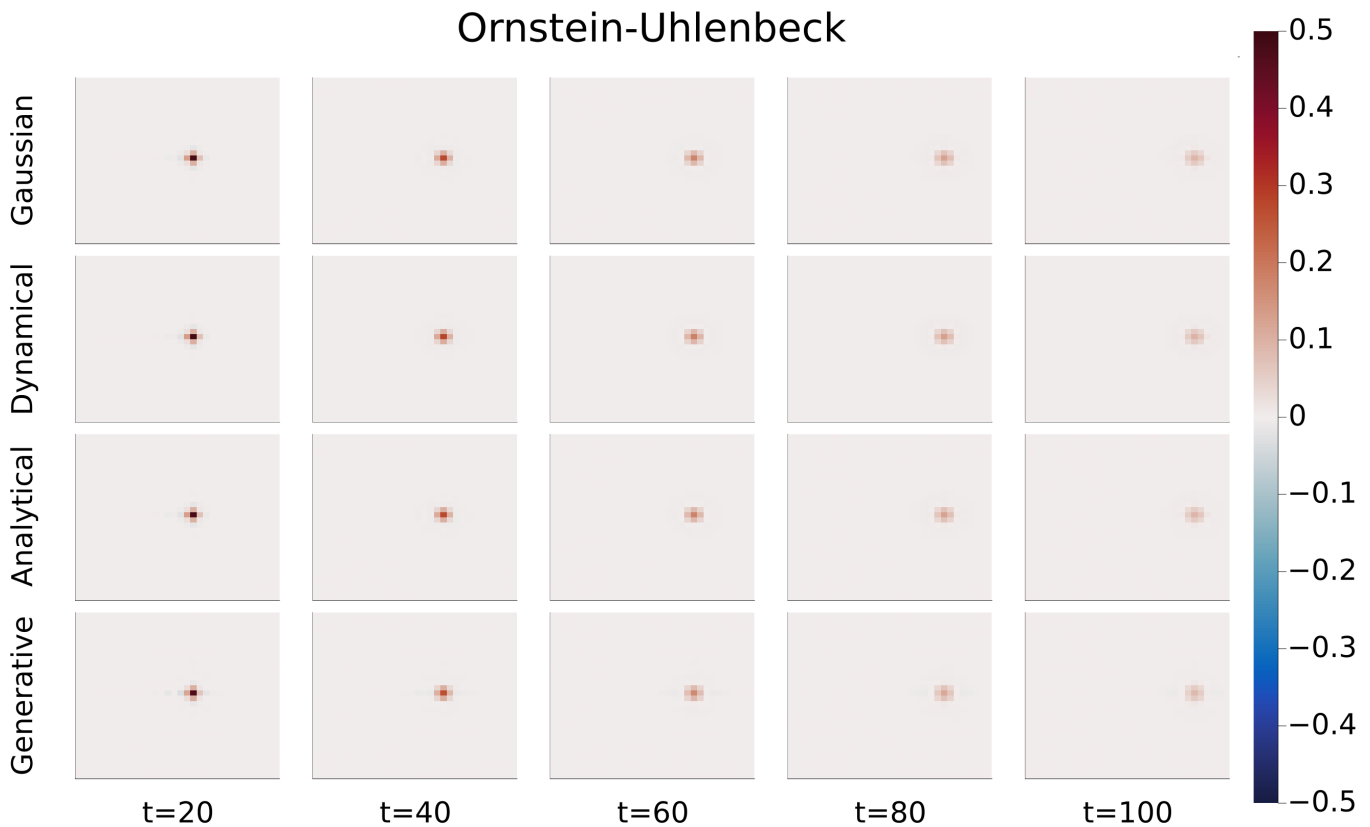


FIG. 11. Colormap of the Ornstein-Uhlenbeck system response for different values of the time parameter t .

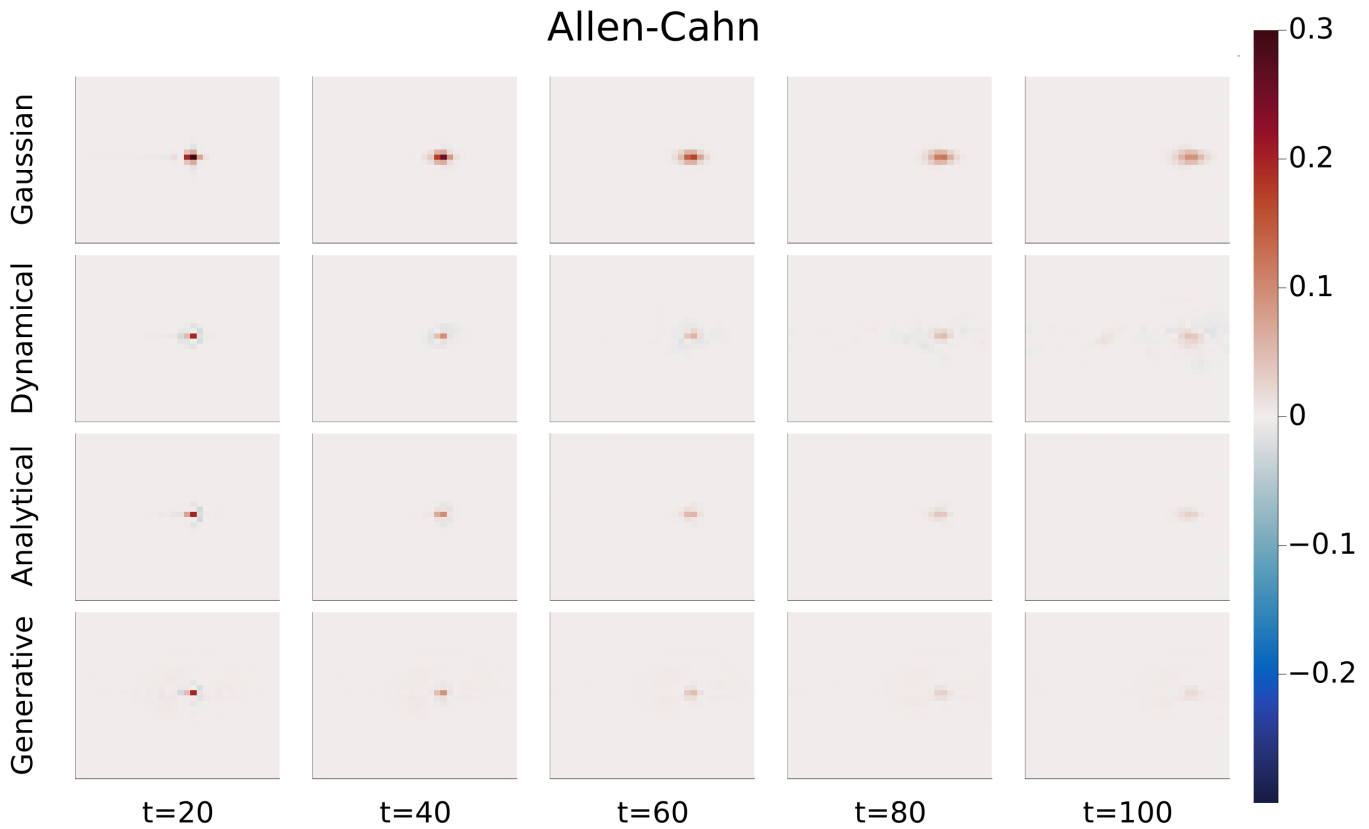


FIG. 12. Colormap of the Allen-Cahn system response for different values of the time parameter t .

where $F = 18.75$, $\nu_f = 0.9/(2\pi)^2$, \mathcal{F}^{-1} is the default discrete inverse Fourier-Transform from FFTW, $\iota = \sqrt{-1}$, and a_i is a filter with the subscript looping over all wavenumbers. Specifically, $a_i = 1$ if $|\vec{k}_i| \leq \sqrt{112.5}$ and $a_i = 0$ otherwise. In our case, the dimensionality of the vector $\vec{\varphi}$ is the same as the Navier-Stokes equation, 32^2 .

* All the authors contributed equally

† ludovico.giorgini@su.se

- [1] P. J. Mucha, T. Richardson, K. Macon, M. A. Porter, and J.-P. Onnela, *Science* **328**, 876 (2010).
- [2] A. Halu, R. J. Mondragón, P. Panzarasa, and G. Bianconi, *PLoS ONE* **8**, e78293 (2013).
- [3] J. Jumper *et al.*, *Nature* **596**, 583 (2021).
- [4] S. L. Brunton, B. R. Noack, and P. Koumoutsakos, *Annual Review of Fluid Mechanics* **52**, 477 (2019).
- [5] J. Barbier, arXiv preprint arXiv:2010.14863 (2020).
- [6] M. F. Singh, C. Wang, M. W. Cole, and S. Ching, arXiv preprint arXiv:2104.02827 (2021).
- [7] S. N. Dorogovtsev, A. V. Goltsev, and J. F. F. Mendes, *Reviews of Modern Physics* **80**, 1275 (2008).
- [8] A.-L. Barabási and R. Albert, *Science* **286**, 509 (1999).
- [9] M. Ghil and V. Lucarini, *Reviews of Modern Physics* **92**, 035002 (2020).
- [10] A. Timmermann, S.-I. An, J.-S. Kug, F.-F. Jin, W. Cai, A. Capotondi, K. M. Cobb, M. Lengaigne, M. J. McPhaden, M. F. Stuecker, *et al.*, *Nature* **559**, 535 (2018).
- [11] Z. Martin, S.-W. Son, A. Butler, H. Hendon, H. Kim, A. Sobel, S. Yoden, and C. Zhang, *Nature Reviews Earth & Environment* **2**, 477 (2021).
- [12] N. Badwan, *Macroeconomic Analysis for Economic Growth*, 145 (2022).
- [13] B. A. Hunt, P. K. Tewarie, A. G. G. Smith, C. Porcaro, K. D. Singh, and P. R. Murphy, *PLOS Biology* [10.1371/journal.pbio.3001686](https://doi.org/10.1371/journal.pbio.3001686) (2021).
- [14] O. Sporns and R. F. Betzel, *Nature Neuroscience* [10.1038/s41593-021-00858-0](https://doi.org/10.1038/s41593-021-00858-0) (2021).
- [15] A. E. BozorgMagham, S. Motesharrei, S. G. Penny, and E. Kalnay, *PLoS ONE* **10**, e0131226 (2015).
- [16] K. Lagemann, C. Lagemann, B. Taschler, and S. Mukherjee, *Nature Machine Intelligence* **5**, 1306 (2023).
- [17] A. Wismüller, A. M. Dsouza, M. A. Vosoughi, and A. Abidin, *Scientific reports* **11**, 7817 (2021).

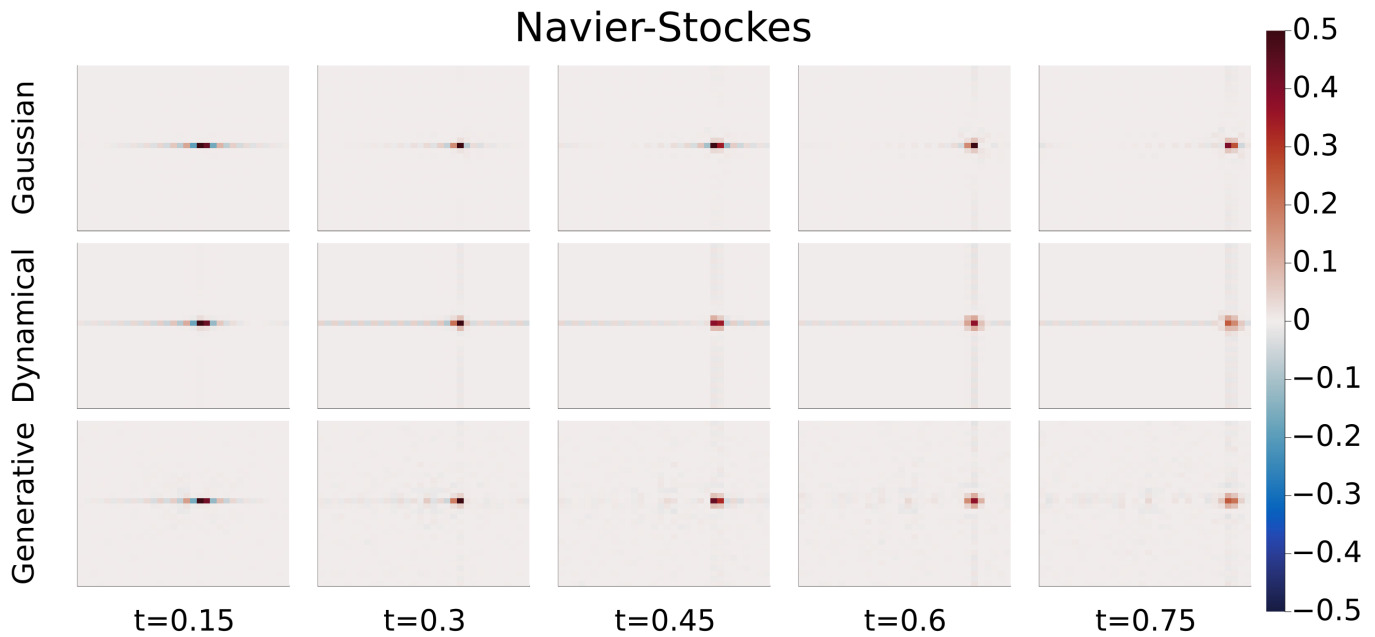


FIG. 13. Colormap of Navier-Stockes system response for different values of the time parameter t .

- [18] N. D. B. Keyes, L. T. Giorgini, and J. S. Wettlaufer, *Chaos: An Interdisciplinary Journal of Nonlinear Science* **33**, 093132 (2023).
- [19] E. Aurell and G. Del Ferraro, in *Journal of Physics: Conference Series*, Vol. 699 (IOP Publishing, 2016) p. 012002.
- [20] R. Friedrich, J. Peinke, M. Sahimi, and M. R. R. Tabar, *Physics Reports* **506**, 87 (2011).
- [21] C. W. Granger, *Econometrica: journal of the Econometric Society*, 424 (1969).
- [22] T. Schreiber, *Physical review letters* **85**, 461 (2000).
- [23] J. Pearl, *Statistics Surveys* **3**, 96 (2009).
- [24] G. Camps-Valls, A. Gerhardus, U. Ninad, G. Varando, G. Martius, E. Balaguer-Ballester, R. Vinuesa, E. Diaz, L. Zanna, and J. Runge, arXiv preprint arXiv:2305.13341 (2023).
- [25] J. Kaddour, A. Lynch, Q. Liu, M. J. Kusner, and R. Silva, arXiv preprint arXiv:2206.15475 (2022).
- [26] M. Baldovin, F. Cecconi, A. Provenzale, and A. Vulpiani, *Scientific Reports* **12**, 15320 (2022).
- [27] F. Cecconi, G. Costantini, C. Guardiani, M. Baldovin, and A. Vulpiani, *Physical Biology* **20**, 056002 (2023).
- [28] F. Falasca, P. Perezhogin, and L. Zanna, *Phys. Rev. E* **109**, 044202 (2024).
- [29] M. Baldovin, F. Cecconi, and A. Vulpiani, *Physical Review Research* **2**, 043436 (2020).
- [30] V. Lucarini, *Journal of Statistical Physics* **173**, 1698 (2018).
- [31] U. M. B. Marconi, A. Puglisi, L. Rondoni, and A. Vulpiani, *Physics reports* **461**, 111 (2008).
- [32] F. Daum, *IEEE Aerospace and Electronic Systems Magazine* **20**, 57 (2005).
- [33] P. Sjöberg, P. Lötstedt, and J. Elf, *Computing and Visualization in Science* **12**, 37 (2009).
- [34] F. C. Cooper and P. H. Haynes, *Journal of the Atmospheric Sciences* **68**, 937 (2011).
- [35] C. E. Leith, *Journal of Atmospheric Sciences* **32**, 2022 (1975).
- [36] P. D. Sardeshmukh and P. Sura, *Journal of Climate* **22**, 1193 (2009).
- [37] A. Gritsun and V. Lucarini, *Physica D: Nonlinear Phenomena* **349**, 62 (2017).
- [38] C. Proistosescu, A. Rhines, and P. Huybers, *Geophysical Research Letters* **43**, 5425 (2016).
- [39] P. C. Loikith and J. D. Neelin, *Geophysical Research Letters* **42**, 8577 (2015).
- [40] M. Branicki and A. J. Majda, *Nonlinearity* **25**, 2543 (2012).
- [41] C. Martinez-Villalobos and J. D. Neelin, *Journal of the Atmospheric Sciences* **76**, 3611 (2019).
- [42] N. Kriegeskorte and X.-X. Wei, *Nature Reviews Neuroscience* **22**, 703 (2021).
- [43] P. Vincent, *Neural computation* **23**, 1661 (2011).
- [44] J. Ho, A. Jain, and P. Abbeel, *Advances in neural information processing systems* **33**, 6840 (2020).
- [45] Y. Song and S. Ermon, *Advances in neural information processing systems* **32** (2019).
- [46] Y. Song, J. Sohl-Dickstein, D. P. Kingma, A. Kumar, S. Ermon, and B. Poole, arXiv preprint arXiv:2011.13456 (2020).
- [47] T. Bischoff and K. Deck, arXiv preprint arXiv:2305.01822 (2023).
- [48] J. Stanczuk, G. Batzolis, T. Deveney, and C.-B. Schönlieb, Your diffusion model secretly knows the dimension of the data manifold (2023), arXiv:2212.12611 [cs.LG].
- [49] O. Ronneberger, P. Fischer, and T. Brox, in *Medical Image Computing and Computer-Assisted Intervention—MICCAI 2015: 18th International Conference, Munich, Germany, October 5–9, 2015, Proceedings, Part III 18* (Springer, 2015) pp. 234–241.
- [50] B. Adcock, S. Brugiapaglia, N. Dexter, and S. Moraga, arXiv preprint arXiv:2012.06081 (2020).

- [51] P. Beneventano, P. Cheridito, R. Graeber, A. Jentzen, and B. Kuckuck, arXiv preprint arXiv:2112.14523 (2021).
- [52] A. Gritsun and G. Branstator, *Journal of the atmospheric sciences* **64**, 2558 (2007).
- [53] G. E. Uhlenbeck and L. S. Ornstein, *Physical review* **36**, 823 (1930).
- [54] R. A. Maller, G. Müller, and A. Szimayer, *Handbook of financial time series*, 421 (2009).
- [55] J. E. Griffin and M. F. Steel, *Journal of Econometrics* **134**, 605 (2006).
- [56] T. Frank, A. Daffertshofer, and P. Beek, *Physical Review E* **63**, 011905 (2000).
- [57] P. Vatiwutipong and N. Phewchean, *Advances in Difference Equations* **2019**, 1 (2019).
- [58] S. M. Allen and J. W. Cahn, *Acta Metallurgica* **20**, 423 (1972).
- [59] A. Kolmogorov, I. Petrovskii, and N. Piskunov, *Selected Works of AN Kolmogorov* **1** (1937).
- [60] A. M. Turing, *Bulletin of mathematical biology* **52**, 153 (1990).
- [61] T. Callahan and E. Knobloch, *Physica D: Nonlinear Phenomena* **132**, 339 (1999).
- [62] S. Kondo and T. Miura, *science* **329**, 1616 (2010).
- [63] G. R. Flierl and A. N. Souza, *Journal of Fluid Mechanics* **986**, A8 (2024).
- [64] A. J. Majda, B. Gershgorin, and Y. Yuan, *Journal of the Atmospheric Sciences* **67**, 1186 (2010).
- [65] B. Gershgorin and A. J. Majda, *Physica D: Nonlinear Phenomena* **239**, 1741 (2010).
- [66] A. J. Majda and D. Qi, *Chaos: An Interdisciplinary Journal of Nonlinear Science* **29**, 103131 (2019), https://pubs.aip.org/aip/cha/article-pdf/doi/10.1063/1.5118690/14624899/103131_1_online.pdf.
- [67] A. N. Souza and M. Tao, *European Journal of Applied Mathematics* **30**, 830–852 (2019).
- [68] I. Corwin and H. Shen, *Bulletin of the American Mathematical Society* **57**, 409 (2020).
- [69] J. Sohl-Dickstein, E. Weiss, N. Maheswaranathan, and S. Ganguli, in *International conference on machine learning* (PMLR, 2015) pp. 2256–2265.
- [70] Y. Song and S. Ermon, *Advances in neural information processing systems* **33**, 12438 (2020).
- [71] B. D. Anderson, *Stochastic Processes and their Applications* **12**, 313 (1982).
- [72] J. Choi, J. Lee, C. Shin, S. Kim, H. Kim, and S. Yoon, in *Proceedings of the IEEE/CVF Conference on Computer Vision and Pattern Recognition* (2022) pp. 11472–11481.
- [73] M. Tancik, P. Srinivasan, B. Mildenhall, S. Fridovich-Keil, N. Raghavan, U. Singhal, R. Ramamoorthi, J. Barron, and R. Ng, *Advances in Neural Information Processing Systems* **33**, 7537 (2020).
- [74] D. P. Kingma and J. Ba, arXiv preprint arXiv:1412.6980 (2014).
- [75] J. P. Boyd, *Chebyshev and Fourier Spectral Methods*, 2nd ed., Dover Books on Mathematics (Dover Publications, Mineola, NY, 2001).